Supplementary Material (ESI) for Journal of Materials Chemistry

Electronic Supplementary Information

J. Mater. Chem.

Effect of asymmetric substitution on the mesomorphic behaviour of low-melting viologen salts of bis(trifluoromethanesulfonyl)amide

Valerio Causin,[a] and Giacomo Saielli[b]

Figures S1: 1H NMR spectrum of 9BPBr. 2

Figures S2: 1H NMR spectrum of 6BP9(Tf_2N)$_2$ ≡ 6BP9. 2

Figures S3: 13C NMR spectrum of 6BP9(Tf_2N)$_2$ ≡ 6BP9. 3

Figures S4: Details of the synthesis and characterization of 8BP9. 4

Figures S5: Details of the synthesis and characterization of 7BP9. 5

Figures S6: Details of the synthesis and characterization of 7BP8. 6

Figures S7: Details of the synthesis and characterization of 6BP8. 7,8

Figures S8: Details of the synthesis and characterization of 5BP8. 9

Figures S9: Details of the synthesis and characterization of 4BP8. 10

Figures S10: Details of the synthesis and characterization of 3BP11. 11

Figures S11: Details of the synthesis and characterization of 4BP11. 12

Figures S12: Details of the synthesis and characterization of 7BP10. 13

Figures S13: Details of the synthesis and characterization of 7BP11. 14

Figures S14: Details of the synthesis and characterization of 8BP11. 15

Figures S15: Details of the synthesis and characterization of 8BP10. 16

Figures S16-S17. TGA of 6BP8. 17

Figure S18. XRD trace of 5BP8. 17

Figures S19-S21. Mosaic textures of 6BP9, 7BP11 and 8BP11. 18

Figures S22-S24. Coloured version of Figures 1, 3 and 9 of the main text. 19

Figures S25. ΔHs of transition of the 8BPn series. 20

Figure S26. ^{1}H and ^{19}F NMR spectra in benzene of 3BP11. 21

Figures S27-S28. Correlation between δ(H) and δ(C) (neat *vs* MeOD solution) of 3BP11. 22

Figure S29. XRD traces of 8BP11 at 50 and 100 °C. 23

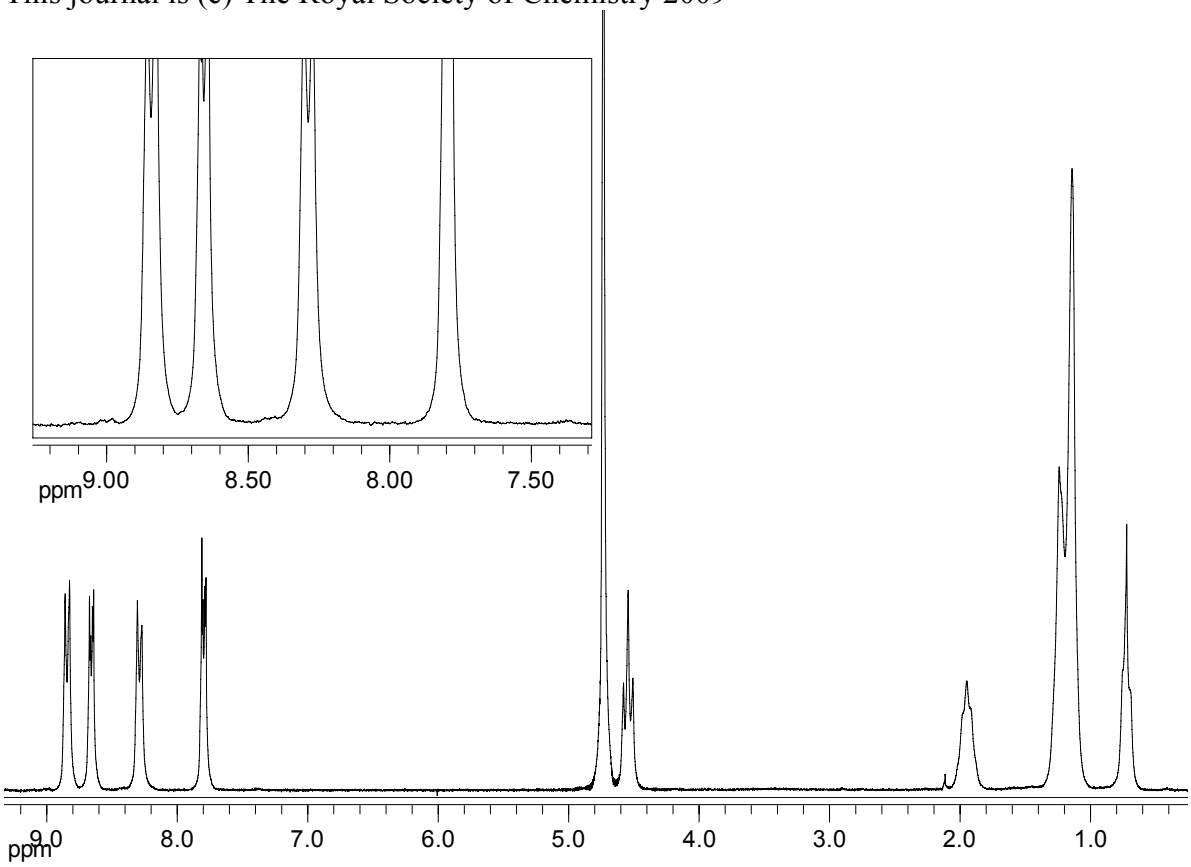

Figure S1. ^{1}H NMR of 9BPBr, D_2O, 200 MHz. Traces of dialkylated product (less than 0.5% mol) can be found at 8.43 and 9.00 ppm.

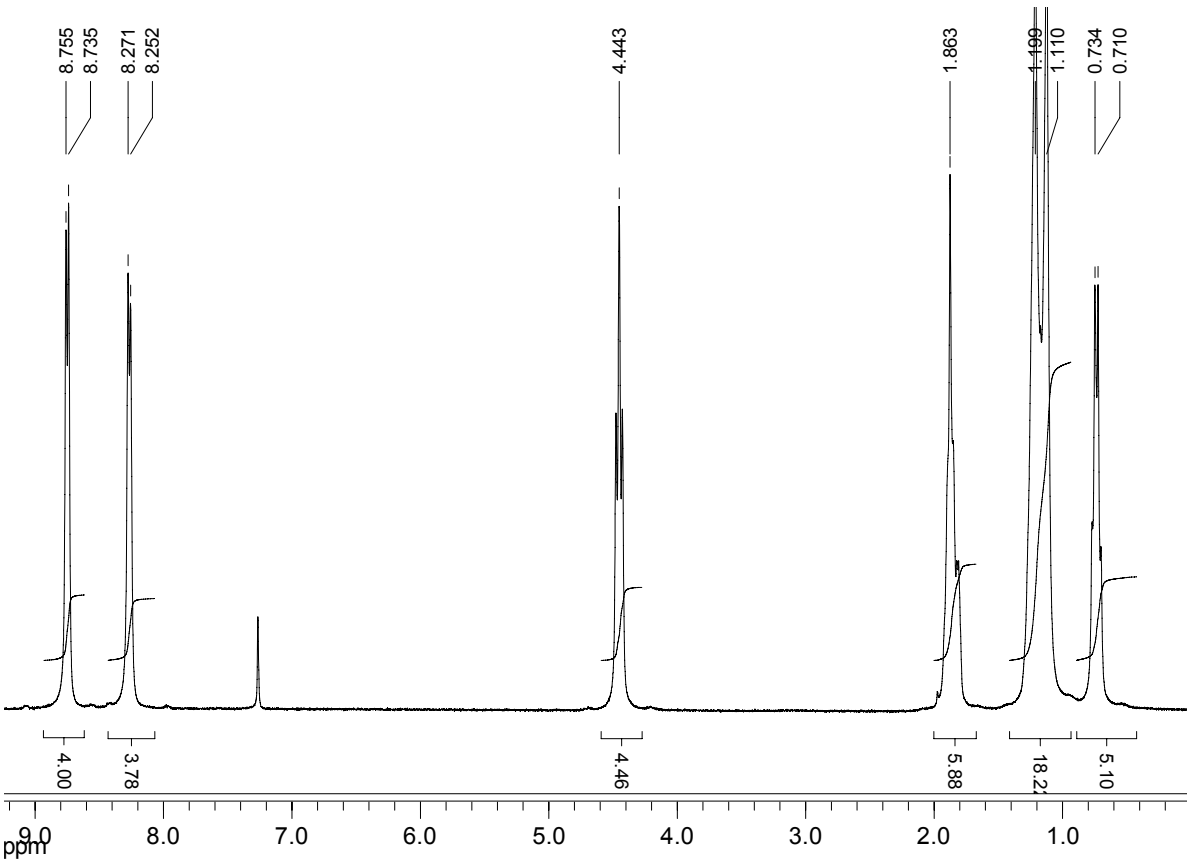

Figure S2. ^{1}H NMR ($CDCl_3$:ACN 3:1, 300 MHz) of 6BP9(Tf_2N)$_2$.

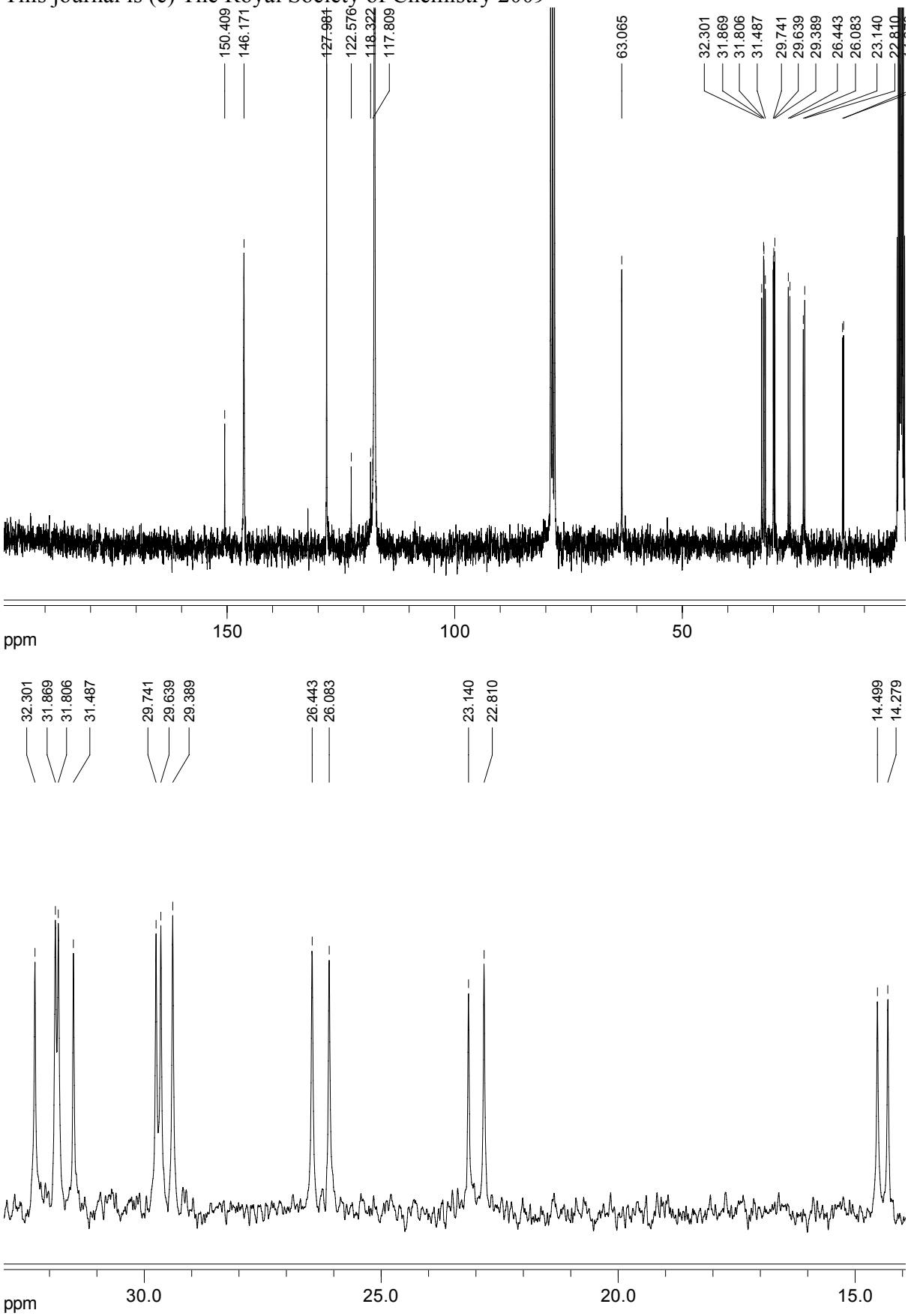

Figure S3. (top) Full ^{13}C NMR ($CDCl_3$:ACN 3:1, 300 MHz) of 6BP9(Tf_2N)$_2$. *C*DCl_3 at 77 ppm, *C*H3CN at 1.7 ppm and CH_3*C*N at 117.5 ppm. (bottom) Aliphatic region.

1-nonyl-1′-octyl-4,4′-bipyridinium di[bis(trifluoromethanesulfonyl)amide], 9BP8(Tf_2N)$_2$.
Synthetic protocol as for the example reported in the Experimental Section of the article. ESI-MS: *m/z* (%) = 198 [M^{2+}] (100), 283 [M-C_8H_{17}]$^+$ (5), 269 [M-C_9H_{19}]$^+$ (5), 280 Tf_2N^-. Elemental analysis: found C 38.64%, H 4.49%, N 5.83%, S 13.12%; calcd C 38.91%, H 4.63%, N 5.85%, S 13.40%.

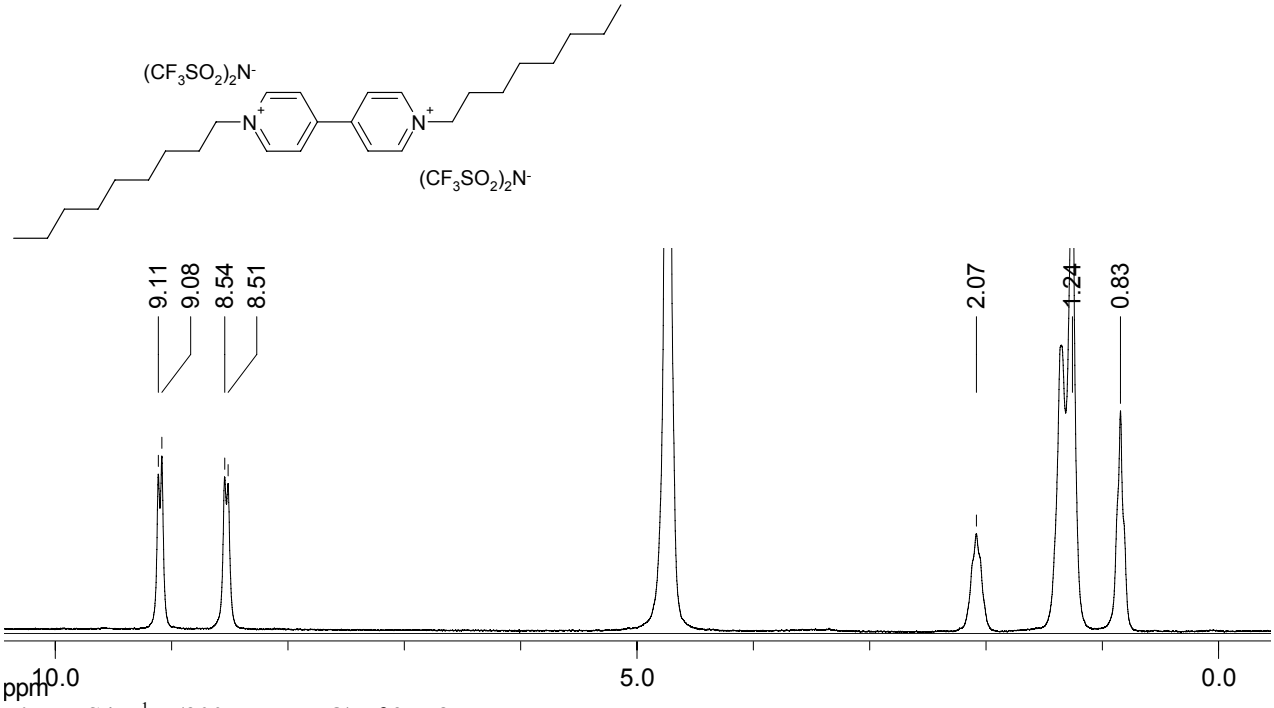

Figure S4a. ^{1}H (200 MHz, D_2O) of 9BP8Br_2.

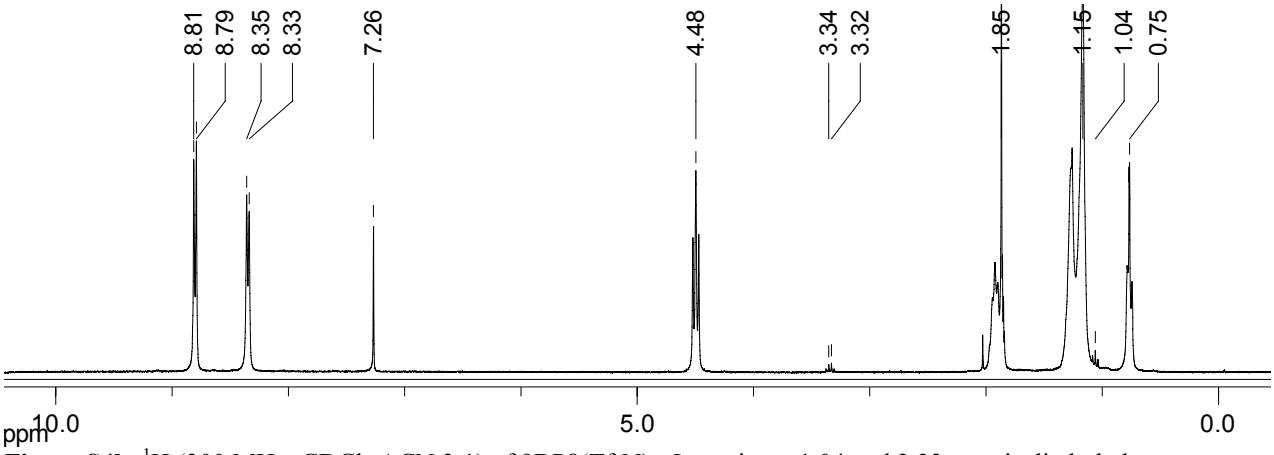

Figure S4b. ^{1}H (300 MHz, $CDCl_3$:ACN 3:1) of 9BP8(Tf_2N)$_2$. Impurity at 1.04 and 3.33 ppm is diethylether.

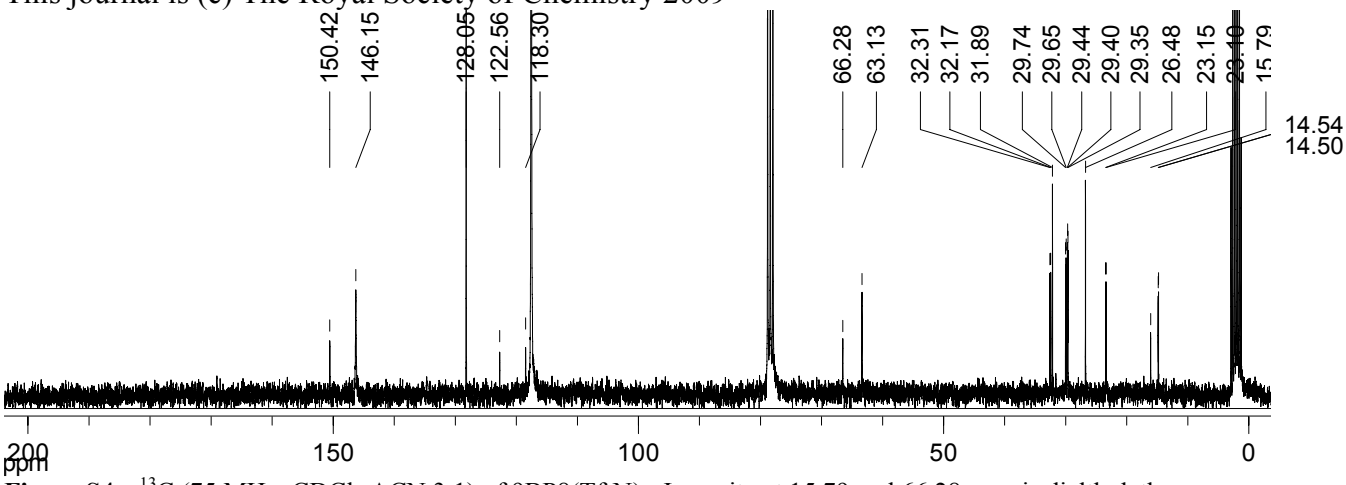

Figure S4c. ^{13}C (75 MHz, $CDCl_3$:ACN 3:1) of 9BP8(Tf_2N)$_2$. Impurity at 15.79 and 66.28 ppm is dielthylether.

1-nonyl-1′-heptyl-4,4′-bipyridinium di[bis(trifluoromethanesulfonyl)amide], 9BP7(Tf_2N)$_2$.

Synthetic protocol as for the example reported in the Experimental Section of the article. ESI-MS: *m*/*z* (%) = 191 [M^{2+}] (100), 283 [M-C_7H_{15}]$^+$ (5), 255 [M-C_9H_{19}]$^+$ (5), 280 Tf_2N^-. Elemental analysis: found C 37.88%, H 4.25%, N 5.88%, S 13.40%; calcd C 38.21%, H 4.49%, N 5.94%, S 13.60%.

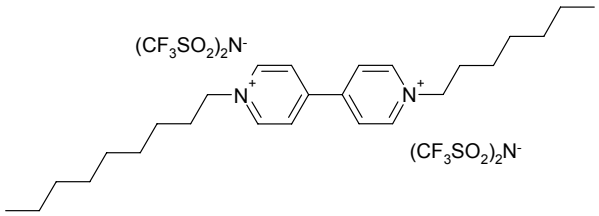

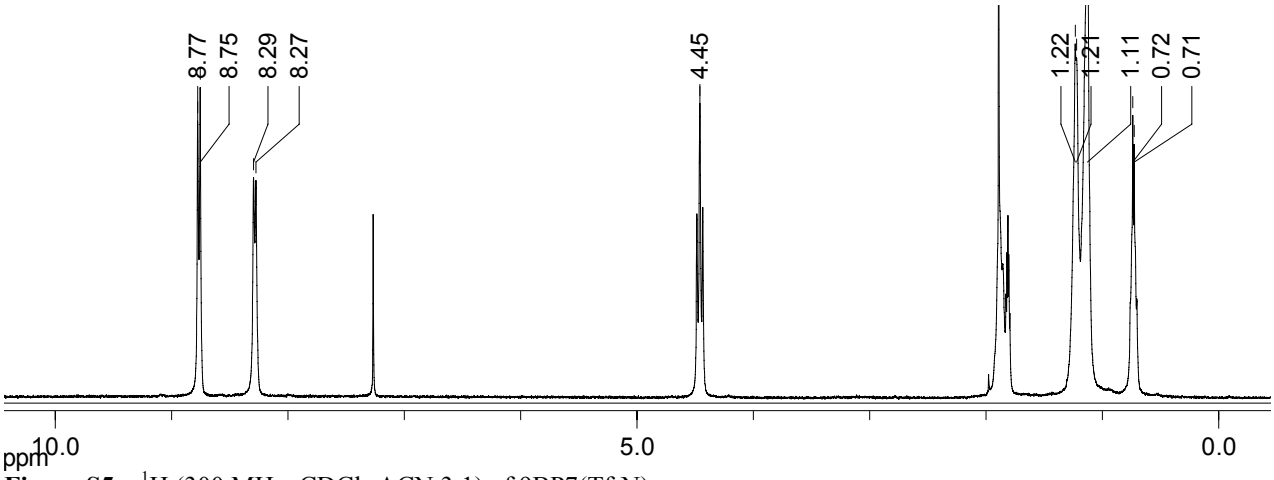

Figure S5a. ^{1}H (300 MHz, $CDCl_3$:ACN 3:1) of 9BP7(Tf_2N)$_2$.

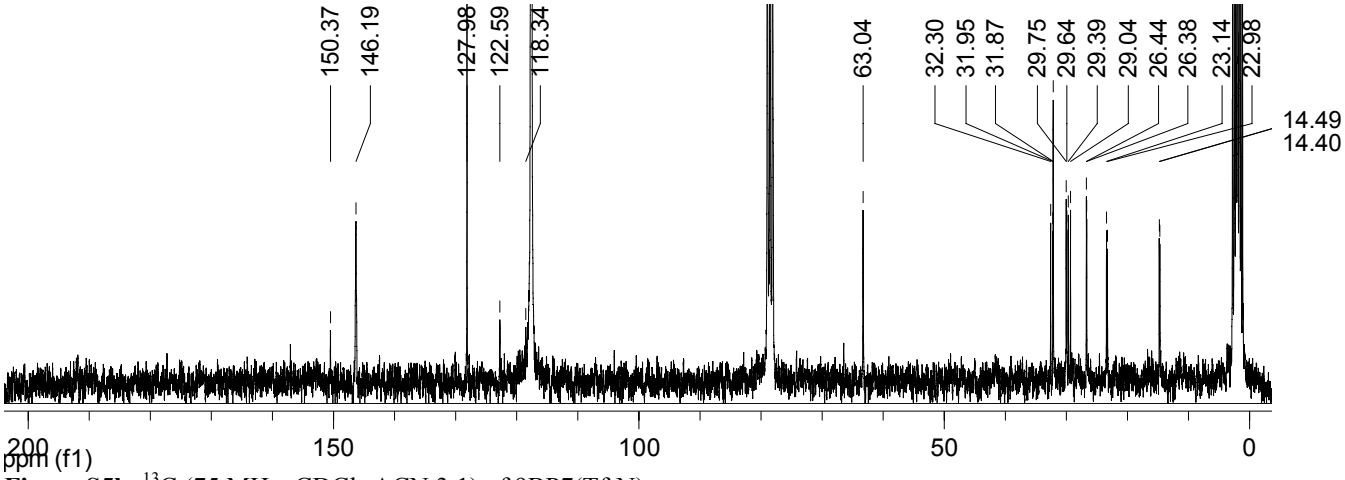

Figure S5b. ^{13}C (75 MHz, $CDCl_3$:ACN 3:1) of 9BP7(Tf_2N)$_2$.

1-octyl-1′-heptyl-4,4′-bipyridinium di[bis(trifluoromethanesulfonyl)amide], 8BP7(Tf_2N)$_2$.

Synthetic protocol as for the example reported in the Experimental Section of the article. Elemental analysis: found C 37.52%, H 4.60%, N 6.04%, S 14.14%; calcd C 37.50%, H 4.34%, N 6.03%, S 13.81%.

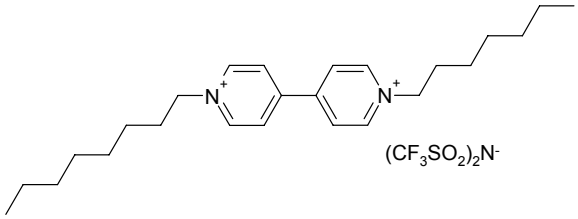

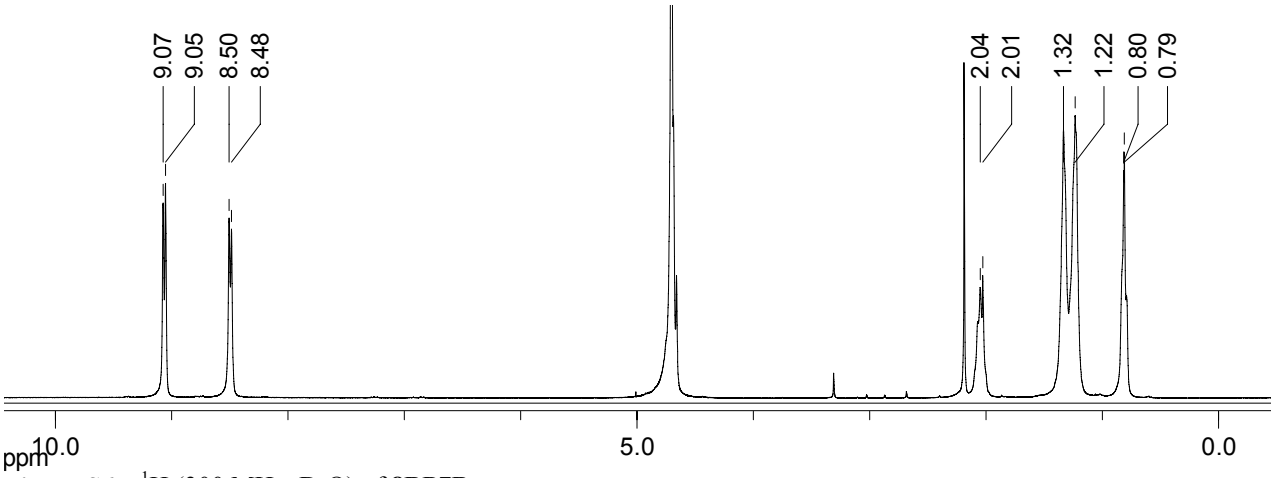

Figure S6a. ^{1}H (300 MHz, D_2O) of **8BP7Br$_2$.**

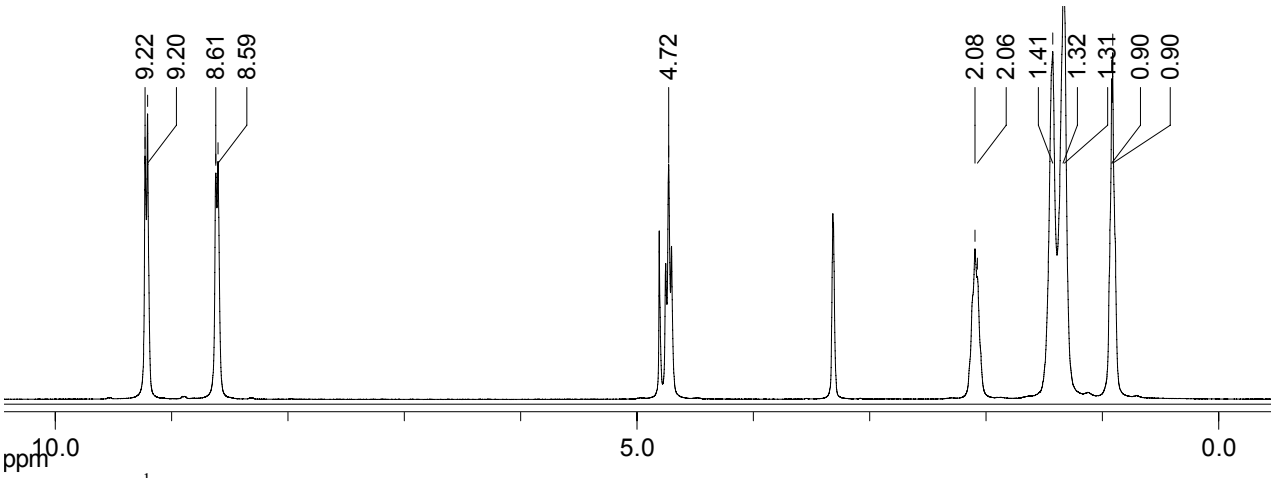

Figure S6b. ^{1}H (300 MHz, MeOD) of **8BP7(Tf_2N)$_2$.**

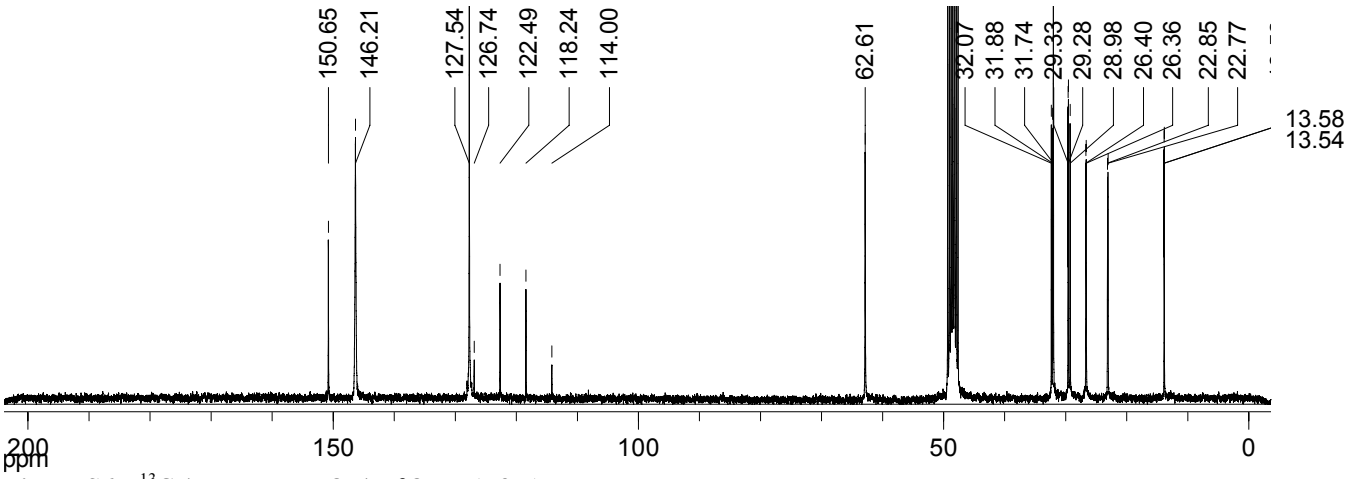

Figure S6c. ^{13}C (75 MHz, MeOD) of **8BP7(Tf_2N)$_2$.**

1-octyl-1′-hexyl-4,4′-bipyridinium di[bis(trifluoromethanesulfonyl)amide], 8BP6(Tf_2N)$_2$.

Synthetic protocol as for the example reported in the Experimental Section of the article. Elemental analysis: found C 36.68%, H 4.37%, N 6.15%, S 14.20%; calcd C 37.76%, H 4.19%, N 6.12%, S 14.02%.

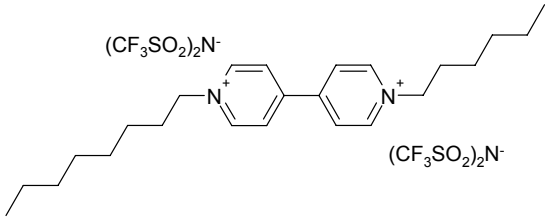

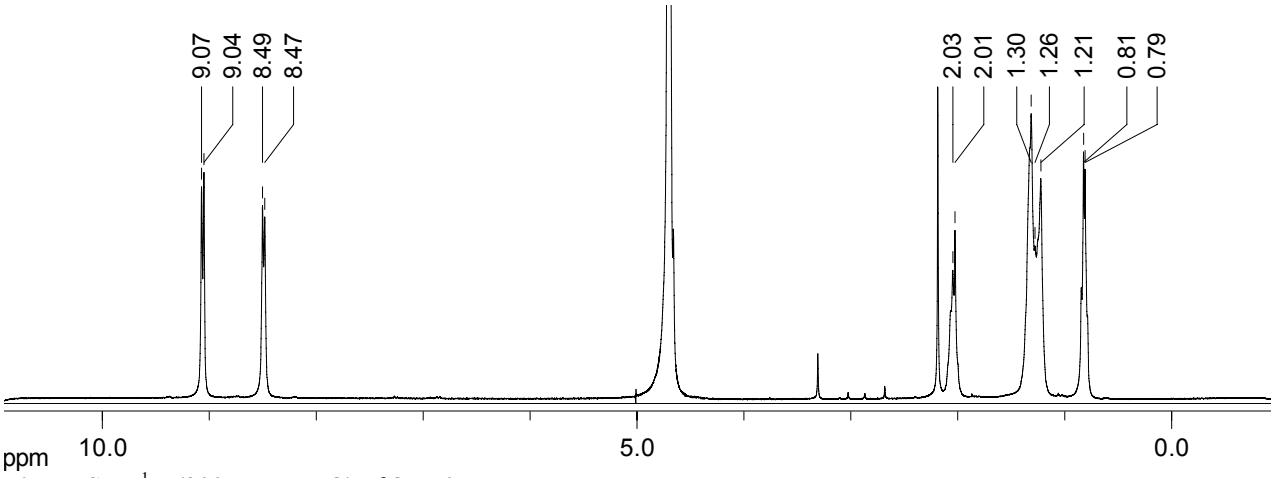

Figure S7a. ^{1}H (300 MHz, D_2O) of **8BP6Br$_2$.**

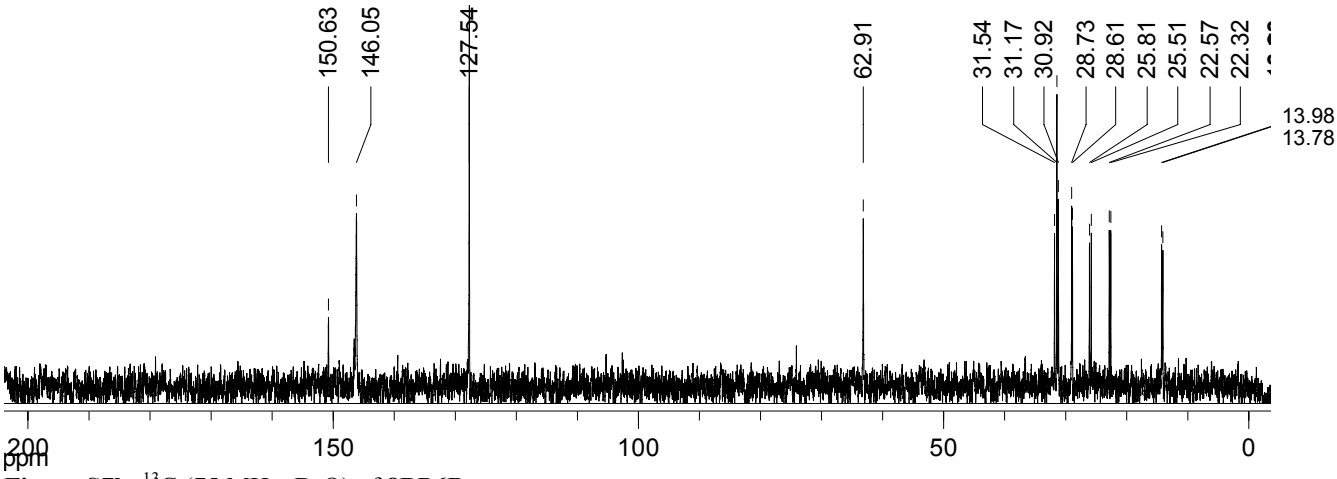

Figure S7b. ^{13}C (75 MHz, D_2O) of **8BP6Br$_2$.**

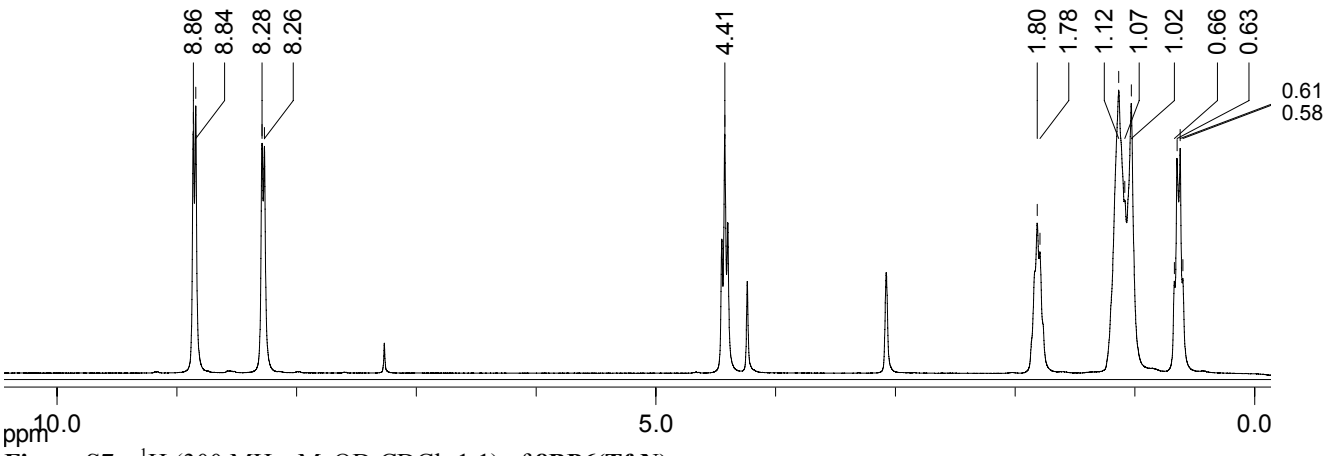

Figure S7c. ^{1}H (300 MHz, MeOD:$CDCl_3$ 1:1) of **8BP6(Tf_2N)$_2$.**

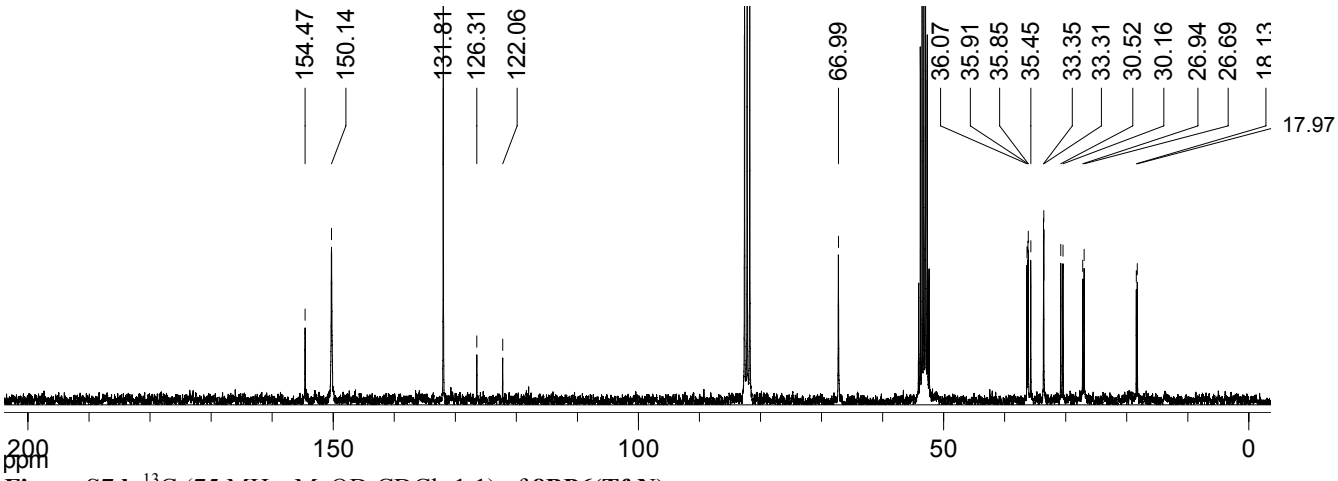

Figure S7d. ^{13}C (75 MHz, MeOD:$CDCl_3$ 1:1) of **8BP6(Tf_2N)$_2$.**

1-octyl-1′-pentyl-4,4′-bipyridinium di[bis(trifluoromethanesulfonyl)amide], 8BP5(Tf_2N)$_2$.

Synthetic protocol as for the example reported in the Experimental Section of the article except the last step: the final product was recovered from water by extraction in dichloromethane since the low melting point did not allow an easy precipitation of the salt. Solvent was then evaporated. Elemental analysis: found C 36.17%, H 4.16%, N 6.32%, S 14.45%; calcd C 36.00%, H 4.03%, N 6.22%, S 14.24%.

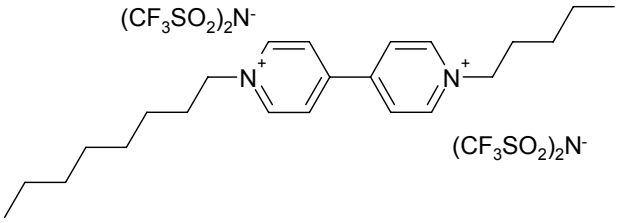

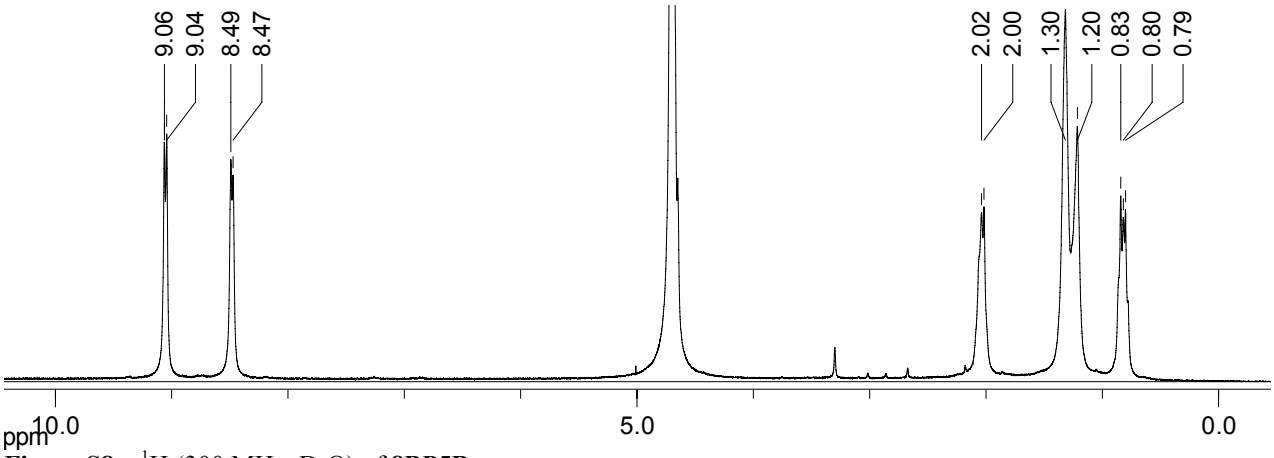

Figure S8a. ^{1}H (300 MHz, D_2O) of **8BP5Br$_2$.**

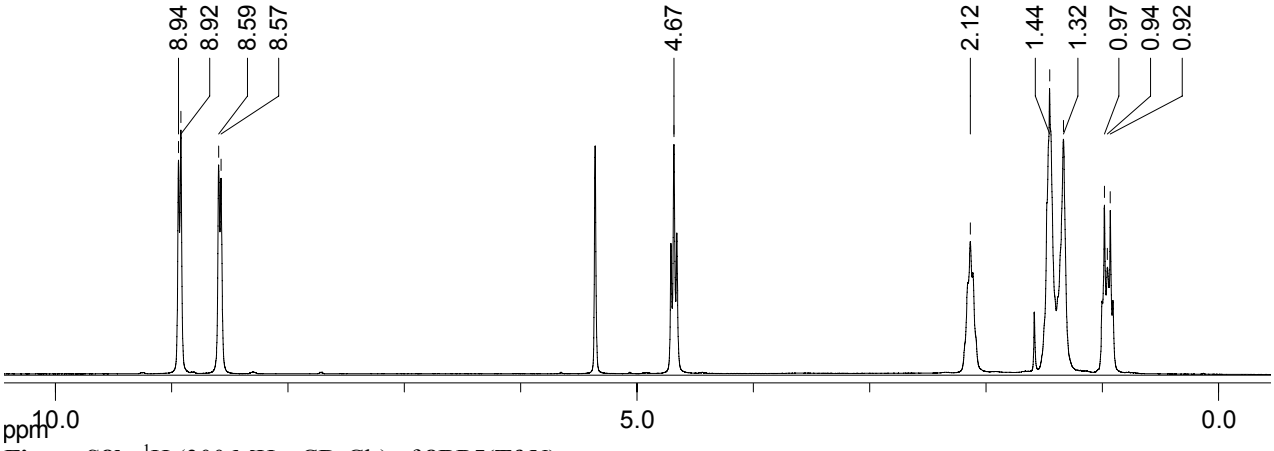

Figure S8b. ^{1}H (300 MHz, CD_2Cl_2) of **8BP5(Tf_2N)$_2$.**

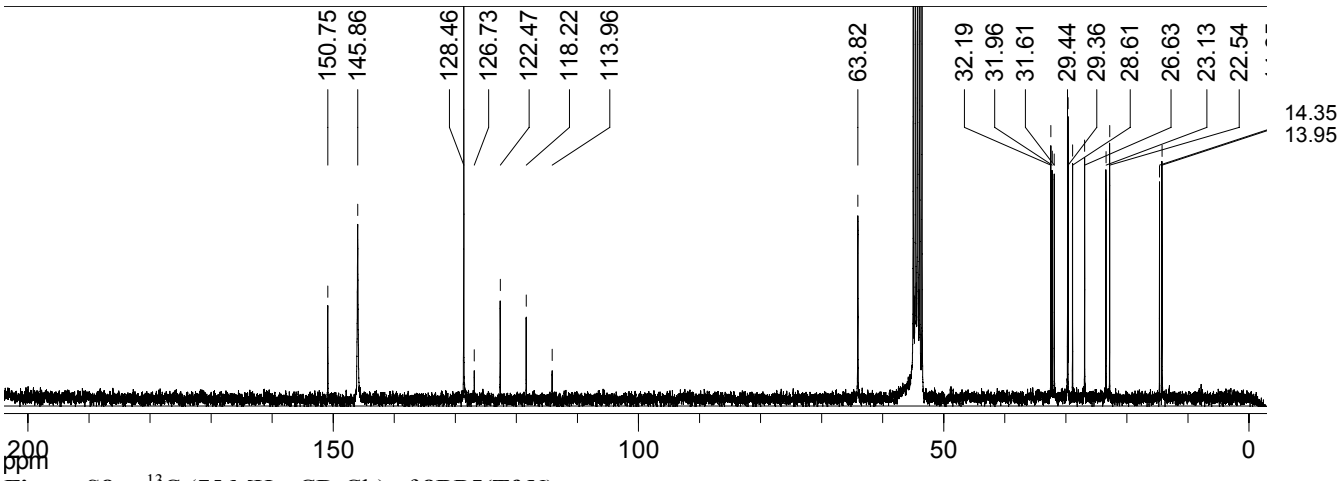

Figure S8c. ^{13}C (75 MHz, CD_2Cl_2) of **8BP5(Tf$_2$N)$_2$.**

1-octyl-1′-butyl-4,4′-bipyridinium di[bis(trifluoromethanesulfonyl)amide], 8BP4(Tf$_2$N)$_2$.

Synthetic protocol as for the example reported in the Experimental Section of the article except the last step: the final product was recovered from water by extraction in dichloromethane since the low melting point did not allow an easy precipitation of the salt. Solvent was then evaporated. Elemental analysis: found C 35.34%, H 4.01%, N 6.29%, S 14.47%; calcd C 35.21%, H 3.86%, N 6.32%, S 14.46%.

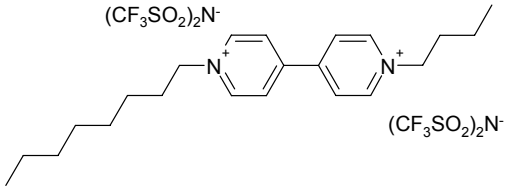

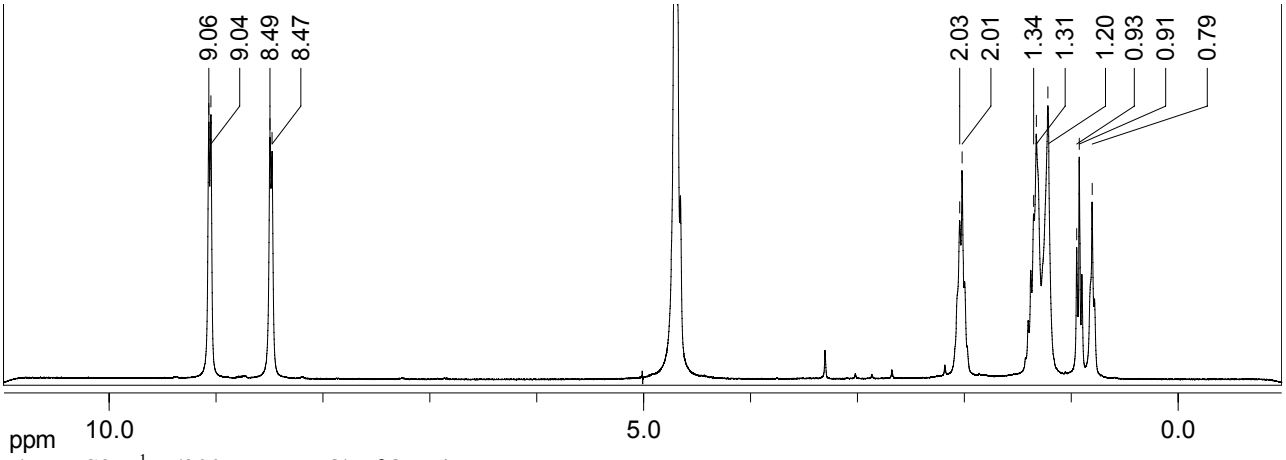

Figure S9a. ^{1}H (300 MHz, D_2O) of **8BP4Br$_2$.**

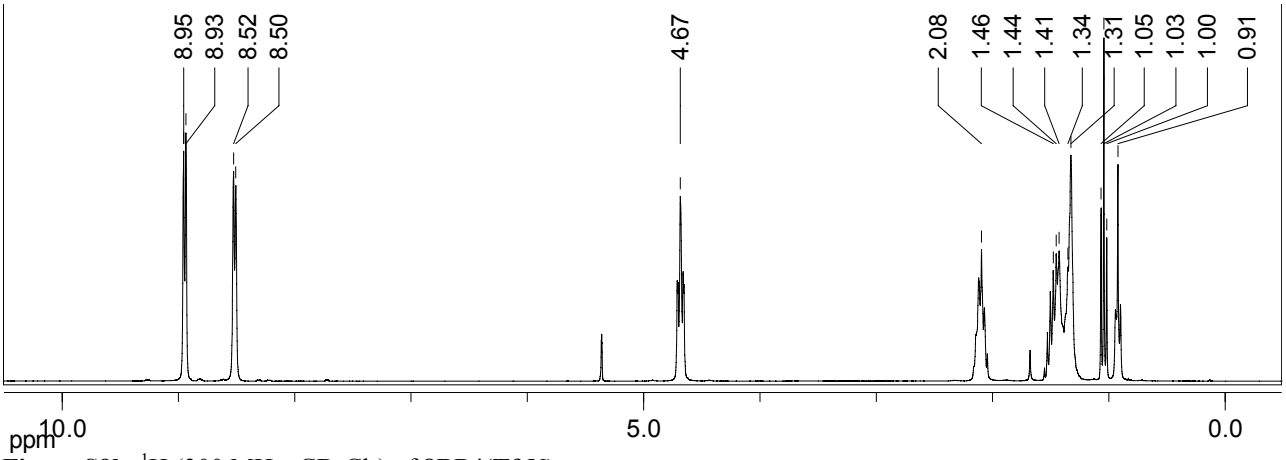

Figure S9b. ^{1}H (300 MHz, CD_2Cl_2) of **8BP4(Tf$_2$N)$_2$.**

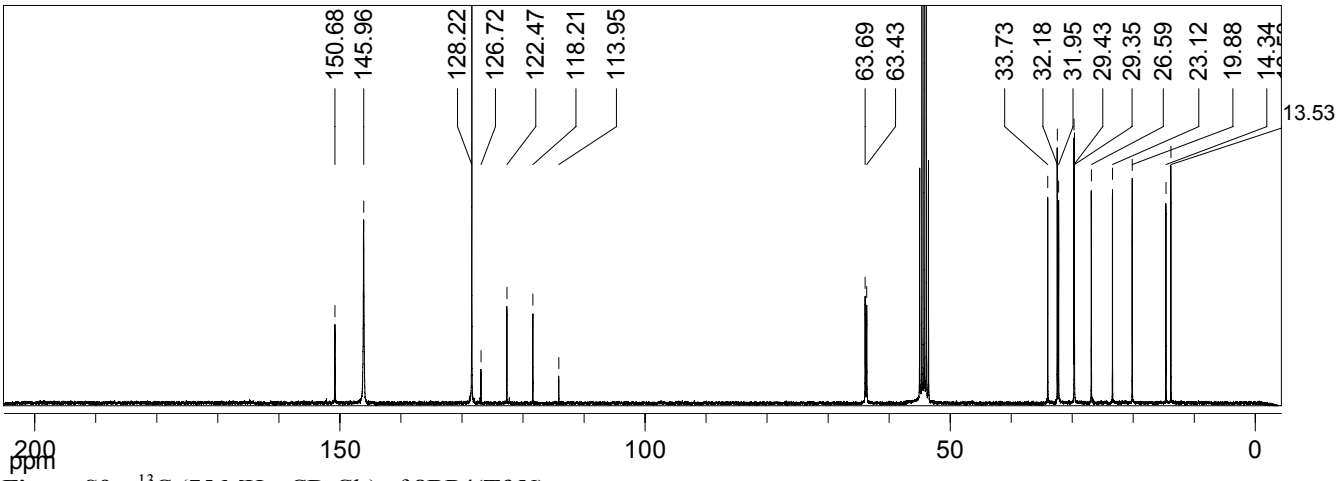

Figure S9c. ^{13}C (75 MHz, CD_2Cl_2) of **8BP4(Tf$_2$N)$_2$.**

1-undecyl-1′-propyl-4,4′-bipyridinium di[bis(trifluoromethanesulfonyl)amide], 11BP3(Tf_2N)$_2$. Synthetic protocol as for the example reported in the Experimental Section of the article except the last step: the final product was recovered from water by extraction in dichloromethane since the low melting point did not allow an easy precipitation of the salt. Solvent was then evaporated.

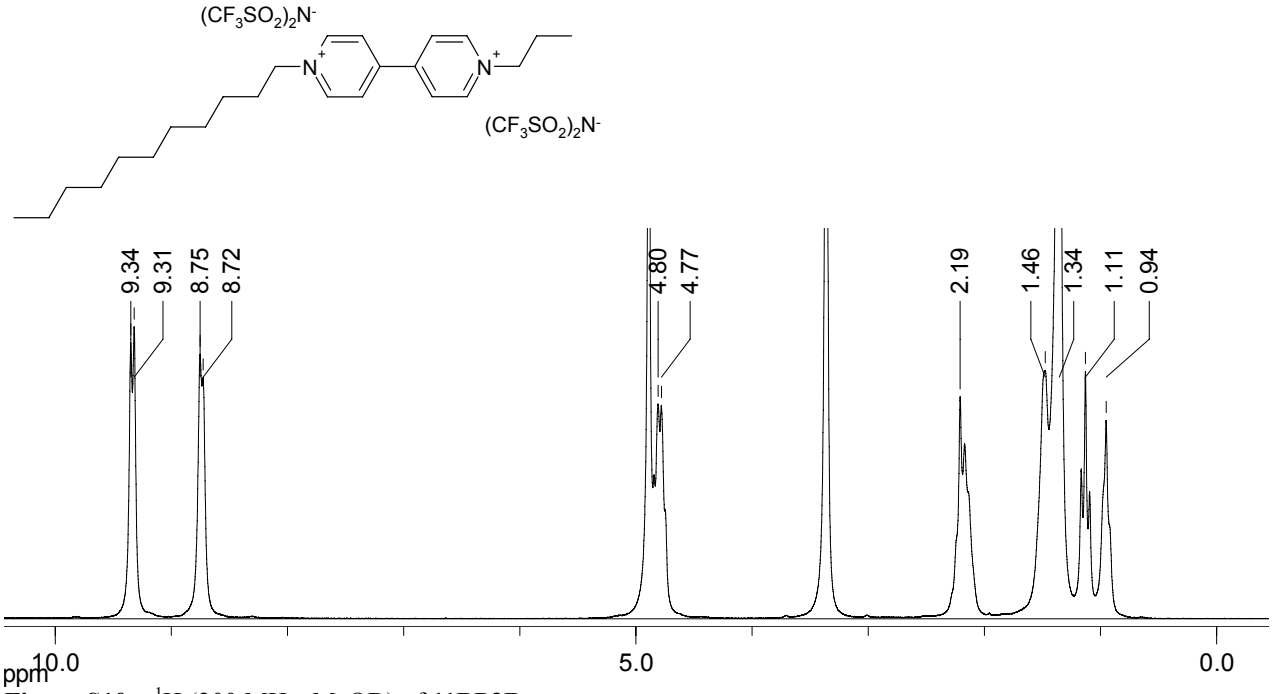

Figure S10a. ^{1}H (200 MHz, MeOD) of **11BP3Br$_2$.**

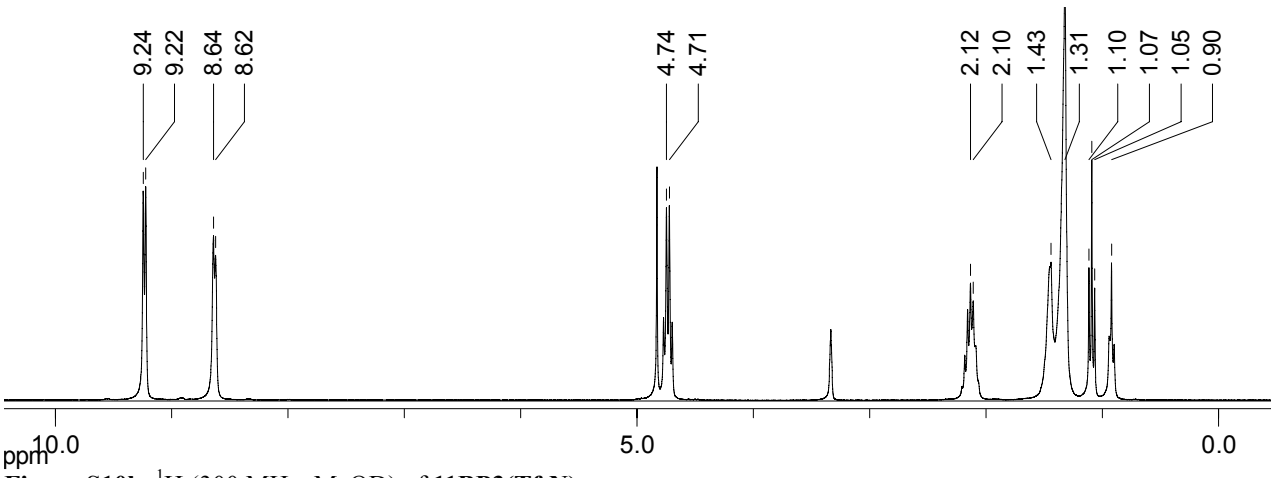

Figure S10b. ^{1}H (300 MHz, MeOD) of **11BP3(Tf_2N)$_2$.**

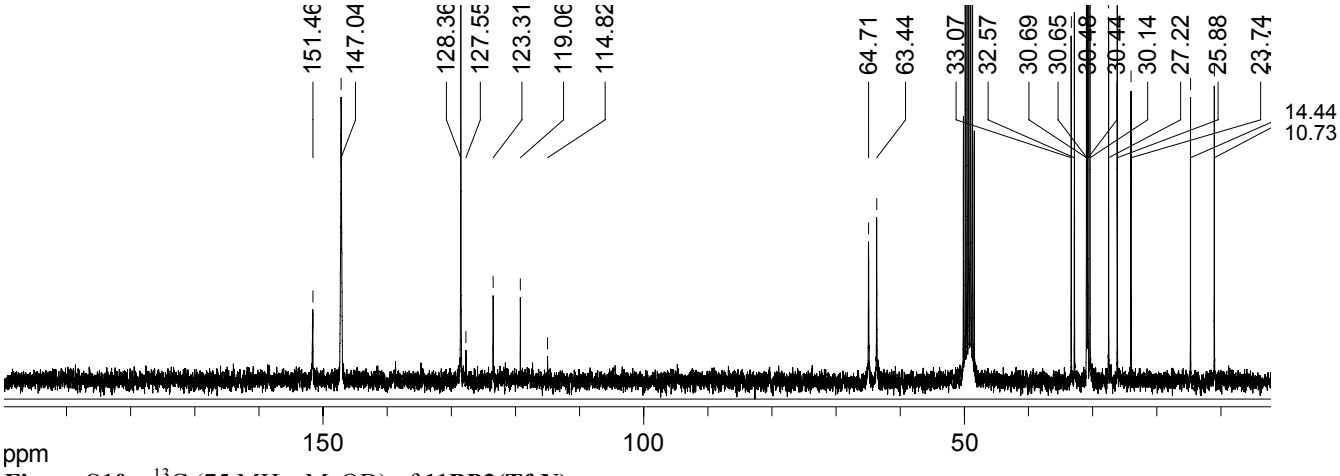

Figure S10c. ^{13}C (75 MHz, MeOD) of **11BP3(Tf$_2$N)$_2$.**

1-undecyl-1′-butylyl-4,4′-bipyridinium di[bis(trifluoromethanesulfonyl)amide], 11BP4(Tf_2N)$_2$.

Synthetic protocol as for the example reported in the Experimental Section of the article except the last step: the final product was recovered from water by extraction in dichloromethane since the low melting point did not allow an easy precipitation of the salt. Solvent was then evaporated

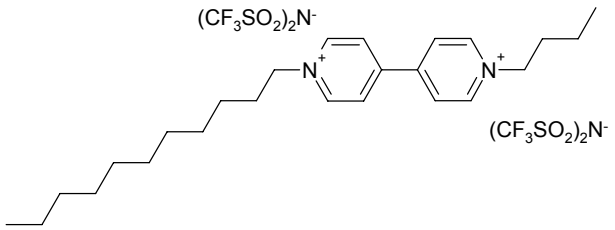

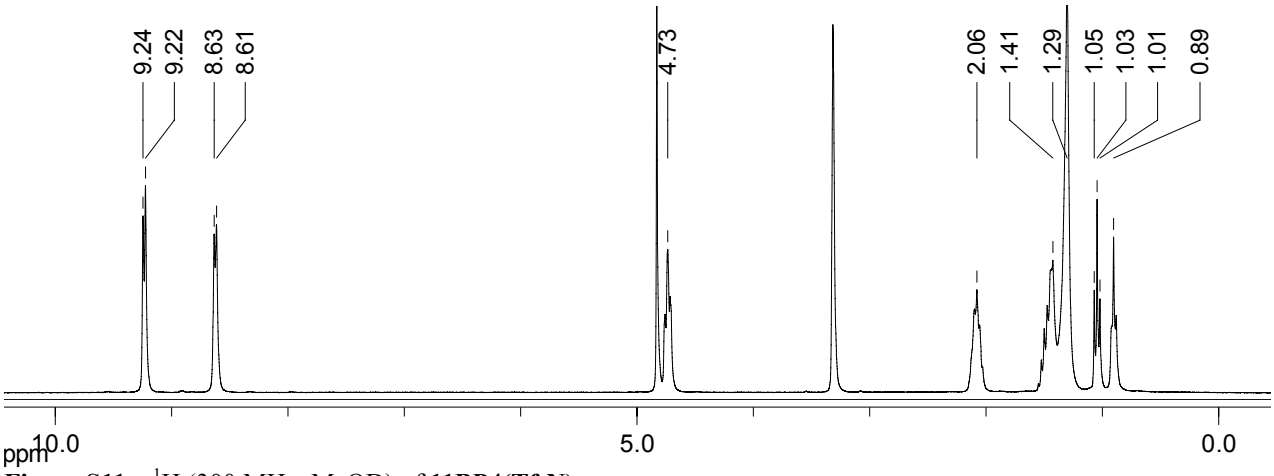

Figure S11a. ^{1}H (300 MHz, MeOD) of **11BP4(Tf_2N)$_2$.**

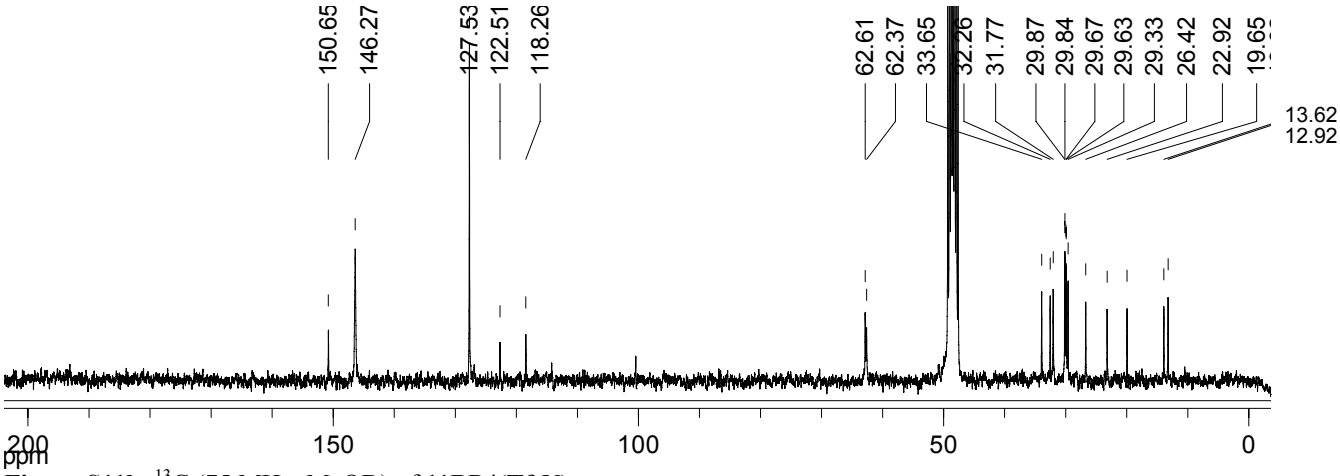

Figure S11b. ^{13}C (75 MHz, MeOD) of **11BP4(Tf_2N)$_2$.**

1-decyl-1′-heptyl-4,4′-bipyridinium di[bis(trifluoromethanesulfonyl)amide], 10BP7(Tf_2N)$_2$.

Synthetic protocol as for the example reported in the Experimental Section of the article. ESI-MS: *m*/*z* (%) = 198 [M^{2+}] (100), 297 [M-C_7H_{15}]$^+$ (5), 255 [M-$C_{10}H_{21}$]$^+$ (5), 280 Tf_2N^-. Elemental analysis: found C 38.72%, H 4.57%, N 5.77%, S 13.22%; calcd C 38.91%, H 4.63%, N 5.85%, S 13.40%.

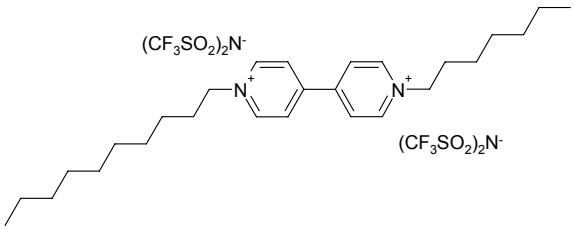

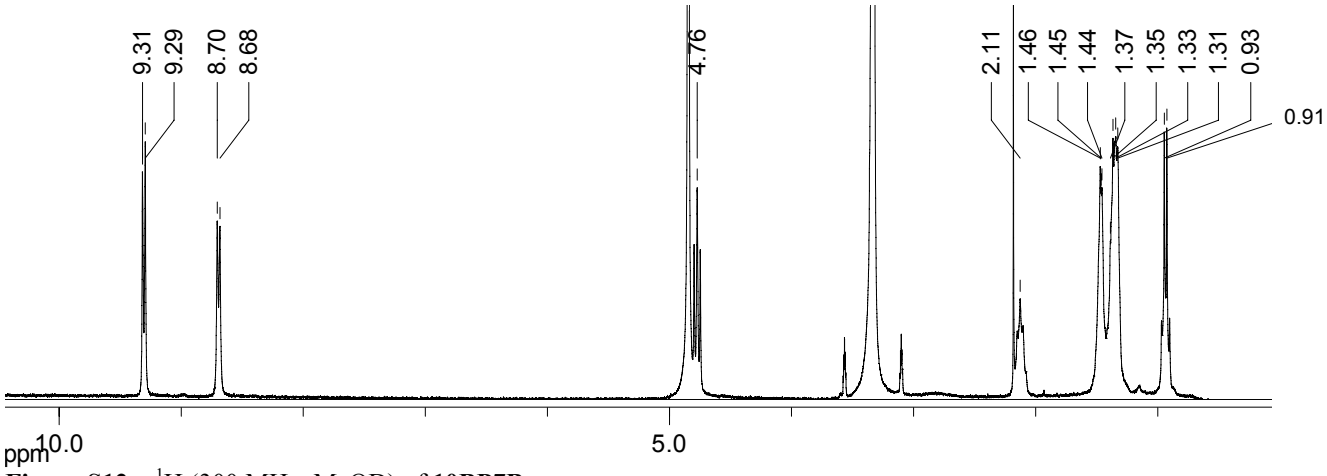

Figure S12a. ^{1}H (300 MHz, MeOD) of **10BP7Br$_2$.**

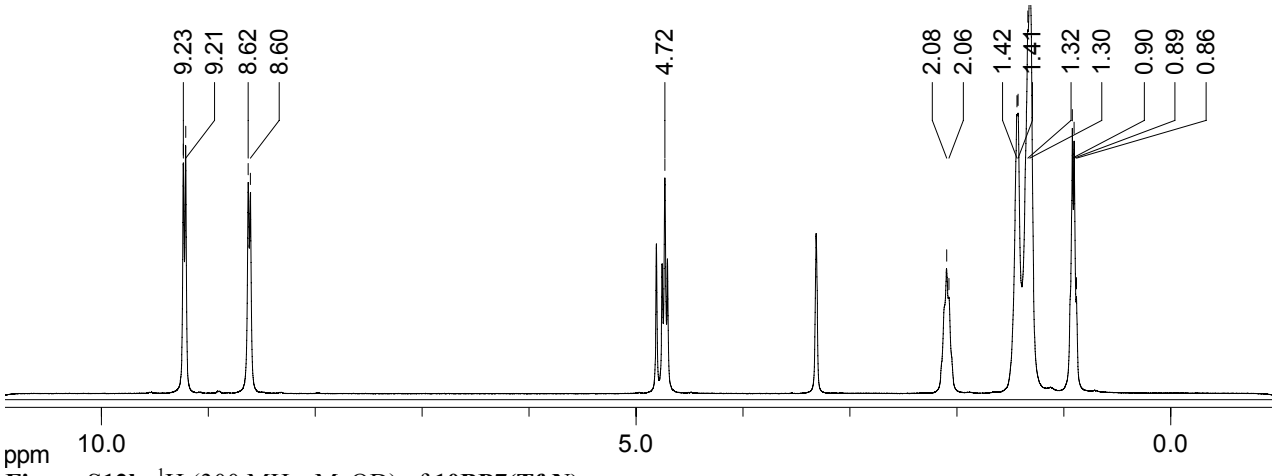

Figure S12b. ^{1}H (300 MHz, MeOD) of **10BP7(Tf_2N)$_2$.**

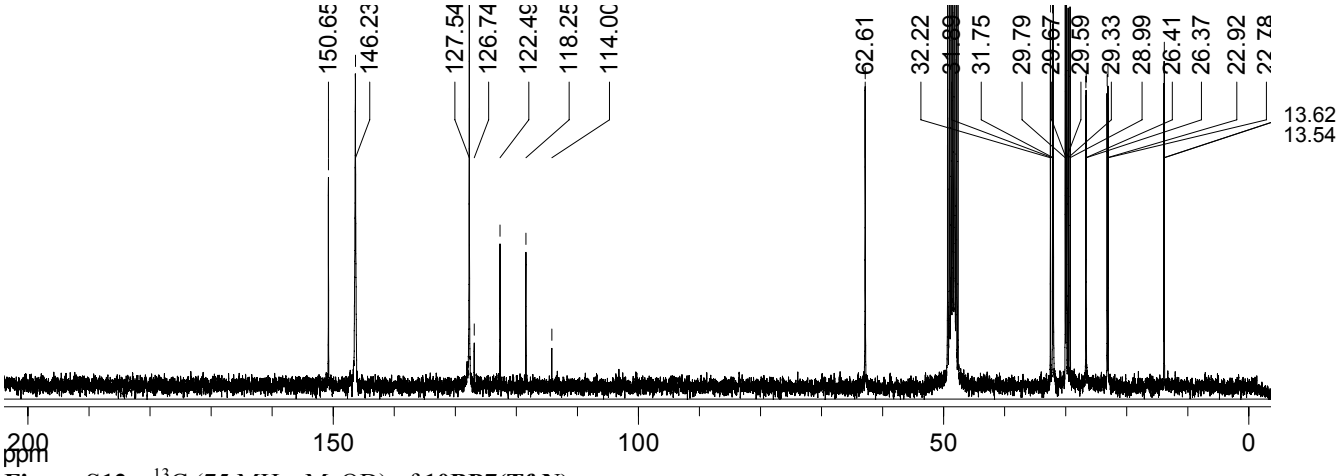

Figure S12c. ^{13}C (75 MHz, MeOD) of **10BP7(Tf$_2$N)$_2$.**

1-undecyl-1′-heptyl-4,4′-bipyridinium di[bis(trifluoromethanesulfonyl)amide], 11BP7(Tf_2N)$_2$.

Synthetic protocol as for the example reported in the Experimental Section of the article. ESI-MS: *m*/*z* (%) = 205 [M^{2+}] (100), 255 [M-$C_{11}H_{23}$]$^+$ (5), 311 [M-C_7H_{15}]$^+$ (5), 280 Tf_2N^-. Elemental analysis: found C 39.47%, H 4.68%, N 5.72%, S 12.95%; calcd C 39.58%, H 4.78%, N 5.77%, S 13.21%.

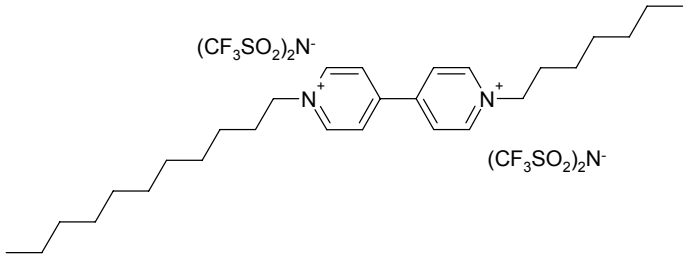

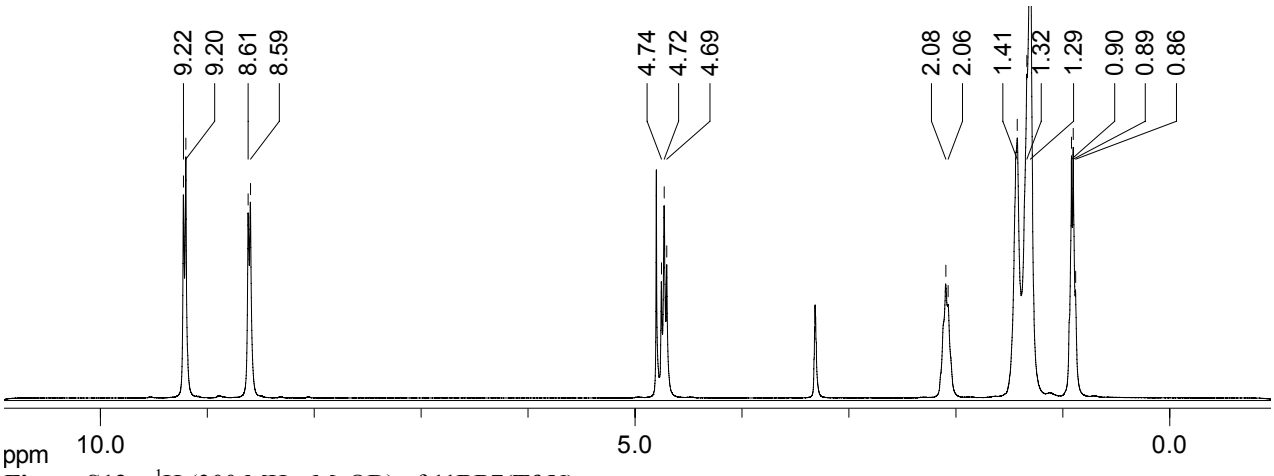

Figure S13a. ^{1}H (300 MHz, MeOD) of **11BP7(Tf_2N)$_2$.**

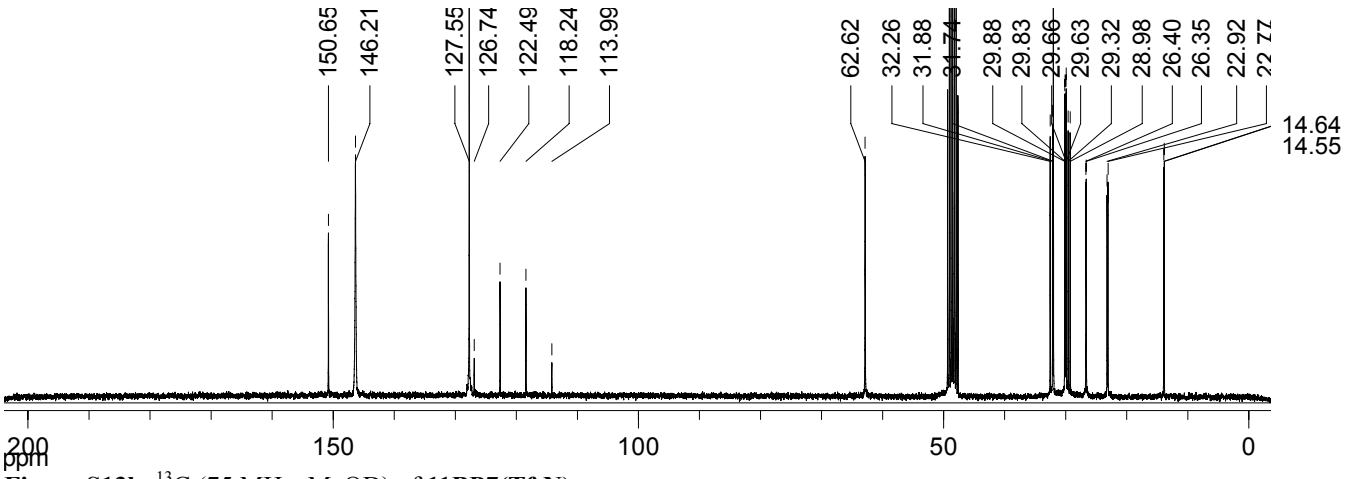

Figure S13b. ^{13}C (75 MHz, MeOD) of **11BP7(Tf_2N)$_2$.**

1-undecyl-1′-octyl-4,4′-bipyridinium di[bis(trifluoromethanesulfonyl)amide], 11BP8(Tf_2N)$_2$.

Synthetic protocol as for the example reported in the Experimental Section of the article.Elemental analysis: found C 40.18%, H 4.95%, N 5.46%, S 13.28%; calcd C 40.24%, H 4.91%, N 5.69%, S 13.02%.

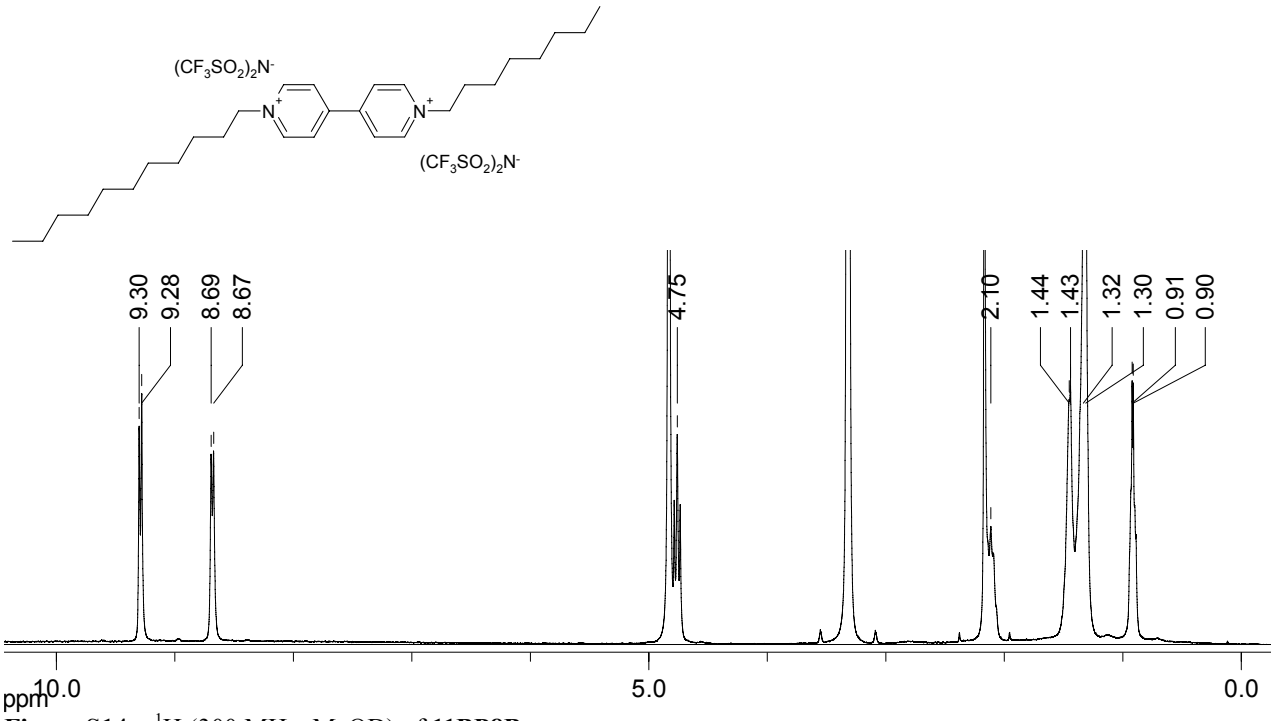

Figure S14a. ^{1}H (300 MHz, MeOD) of **11BP8Br$_2$.**

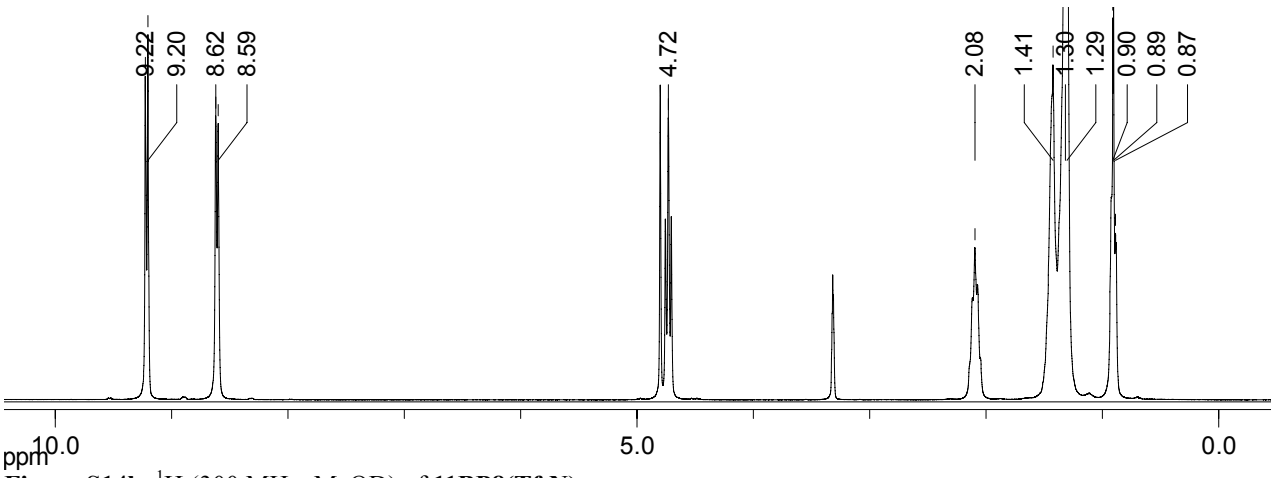

Figure S14b. ^{1}H (300 MHz, MeOD) of **11BP8(Tf_2N)$_2$.**

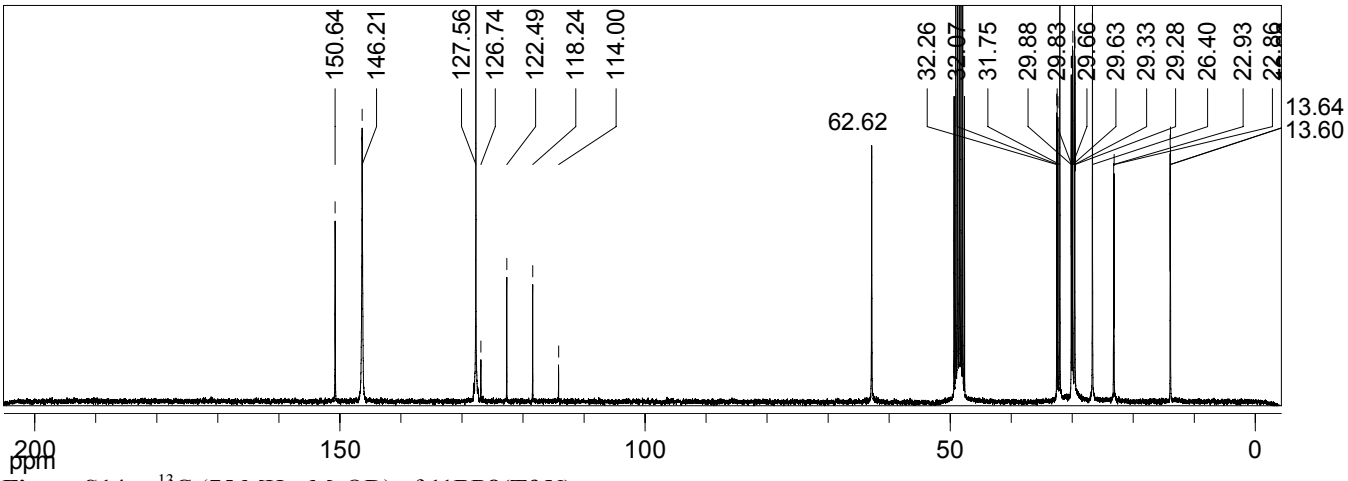

Figure S14c. ^{13}C (75 MHz, MeOD) of **11BP8(Tf$_2$N)$_2$.**

1-decyl-1′-octyl-4,4′-bipyridinium di[bis(trifluoromethanesulfonyl)amide], 10BP8(Tf_2N)$_2$.

Synthetic protocol as for the example reported in the Experimental Section of the article. Elemental analysis: found C 39.81%, H 4.60%, N 5.55%, S 12.91%; calcd C 39.58%, H 4.78%, N 5.77%, S 13.21%.

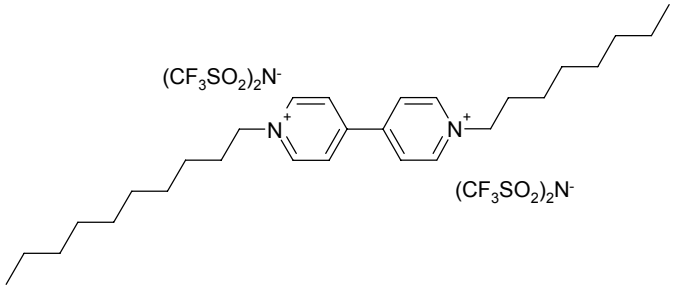

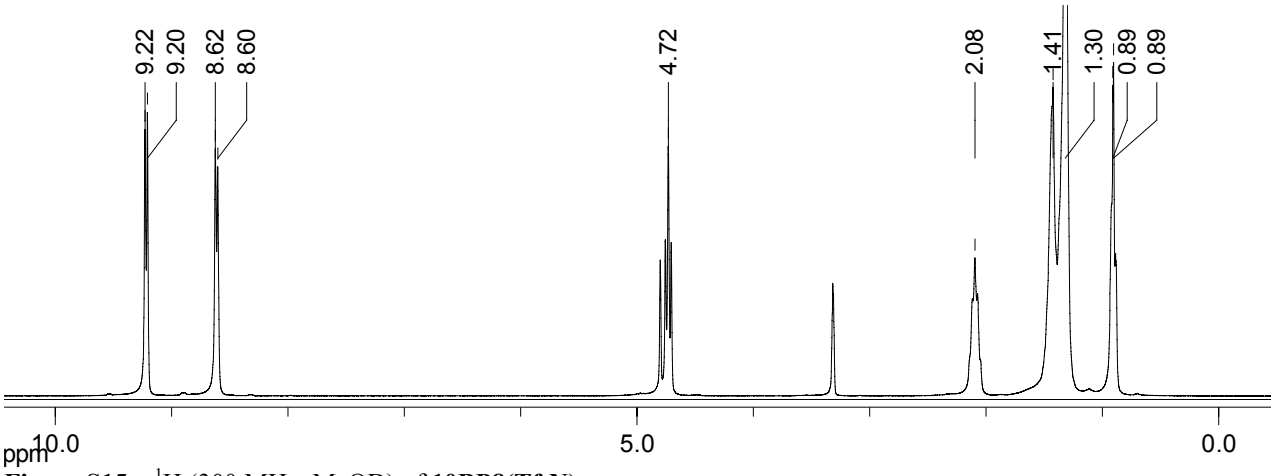

Figure S15a. ^{1}H (300 MHz, MeOD) of **10BP8(Tf_2N)$_2$.**

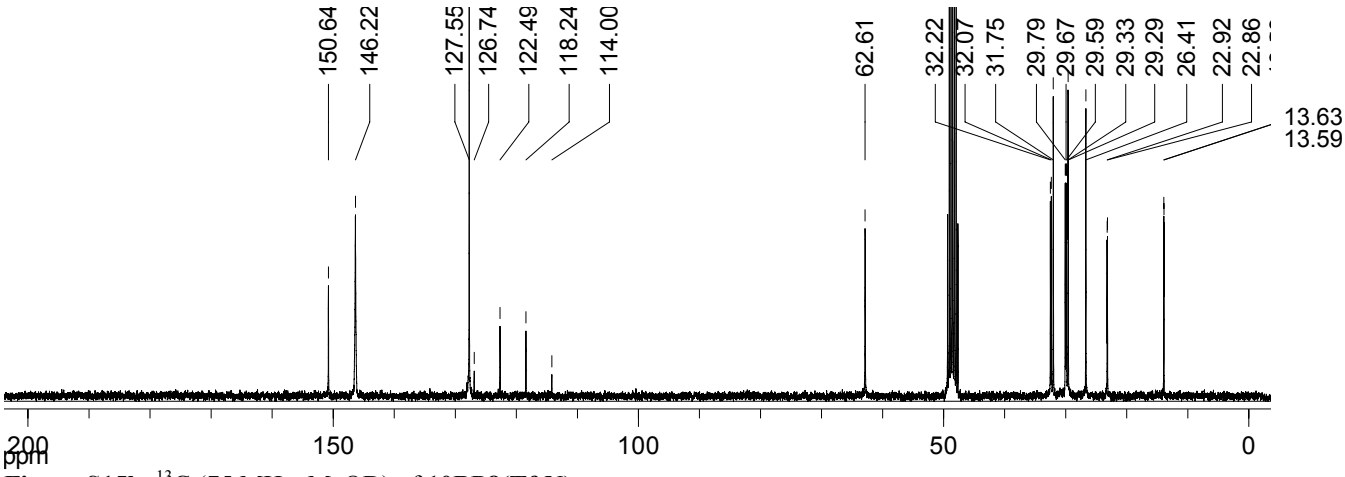

Figure S15b. ^{13}C (75 MHz, MeOD) of **10BP8(Tf_2N)$_2$.**

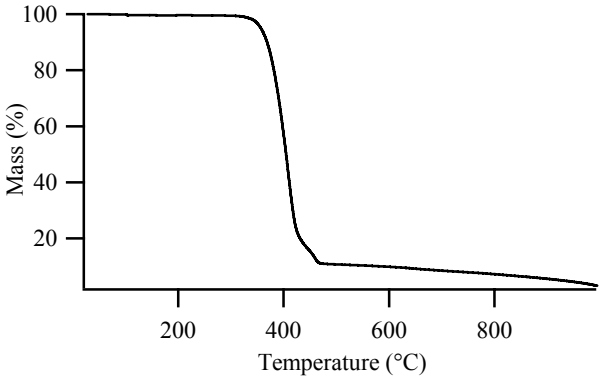

Figure S16. TGA thermogram in nitrogen atmosphere for sample 6BP8

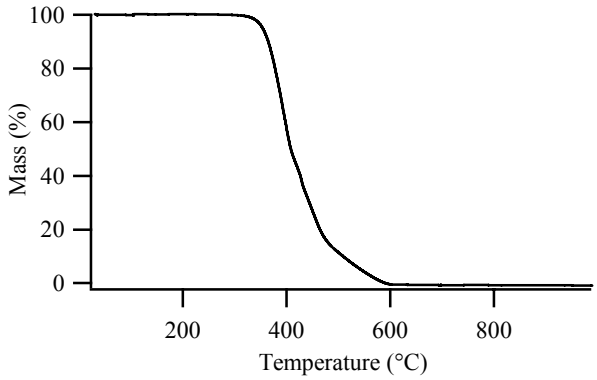

Figure S17. TGA thermogram in air for sample 6BP8

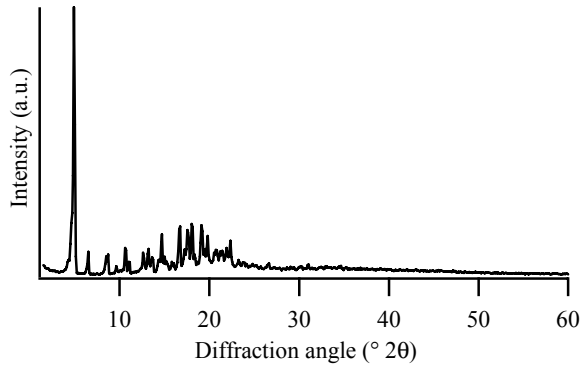

Fig. S18 XRD pattern of sample 5BP8 taken at room temperature.

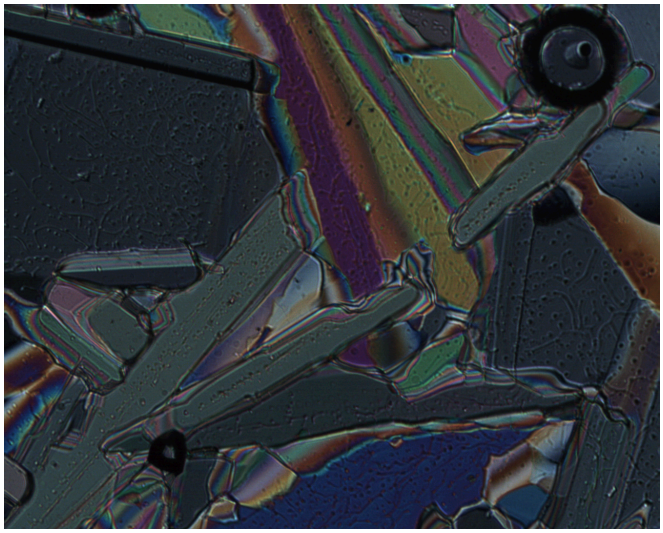

Figure S19. PLOM micrograph of the mosaic textures of 6BP9 at 80 °C after cooling from the melt.

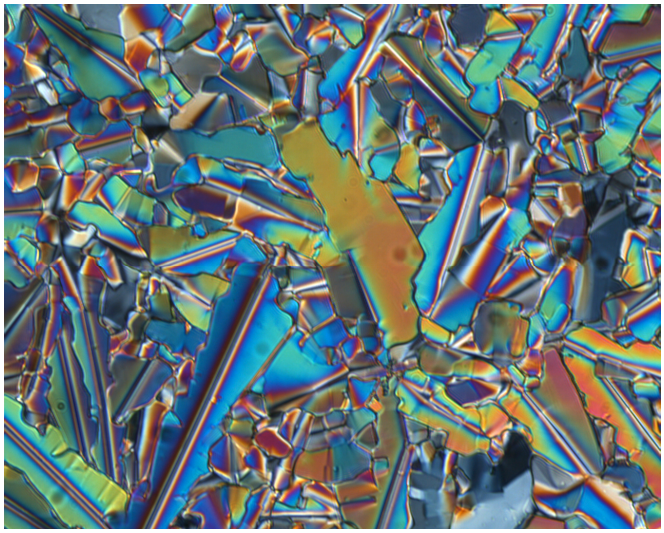

Figure S20. PLOM micrograph of the mosaic textures of 7BP11 at 100 °C after cooling from the melt.

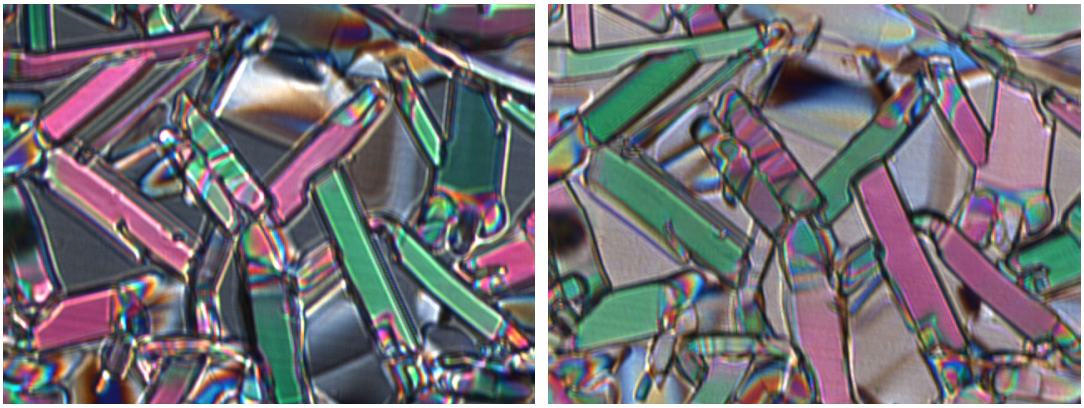

Figure S21. PLOM micrographs of the mosaic textures of 8BP11 at 90 °C after cooling from the melt. (Left) crossed polarisers, (right) parallel polarisers, showing the regions of homeotropic alignment turning from black to white.

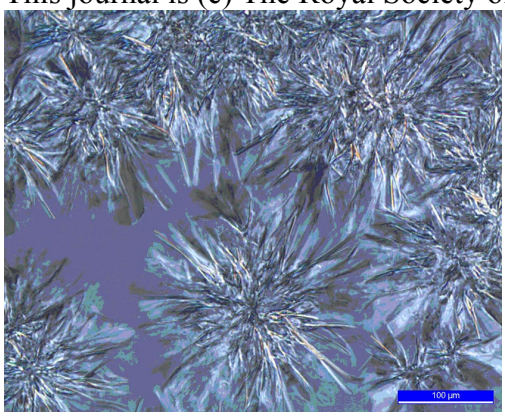

Figure S22. PLOM micrograph of sample 3BP11 taken at 44 °C. The transition from the isotropic melt to the crystalline phase is in its initial stage showing the growth of spherulites (coloured version of Figure 1).

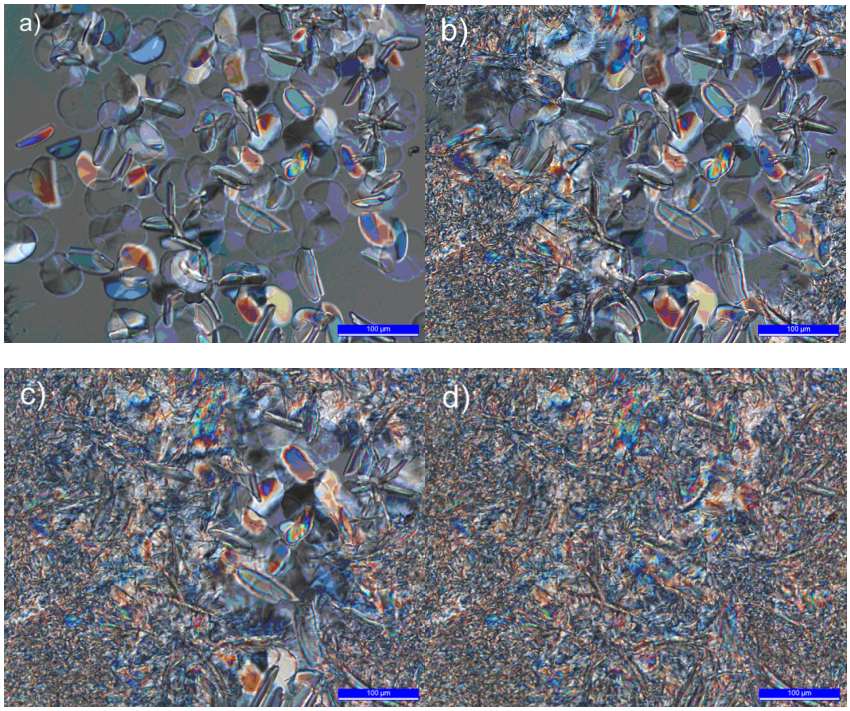

Figure S23. Snapshots taken by PLOM during an isothermal at 30 °C after cooling from the melt of sample 4BP11. a) after 10 minutes, b) after 20 minutes, c) after 40 minutes and d) after 1 hour. The metric bar corresponds to 100 µm (coloured version of Figure 3).

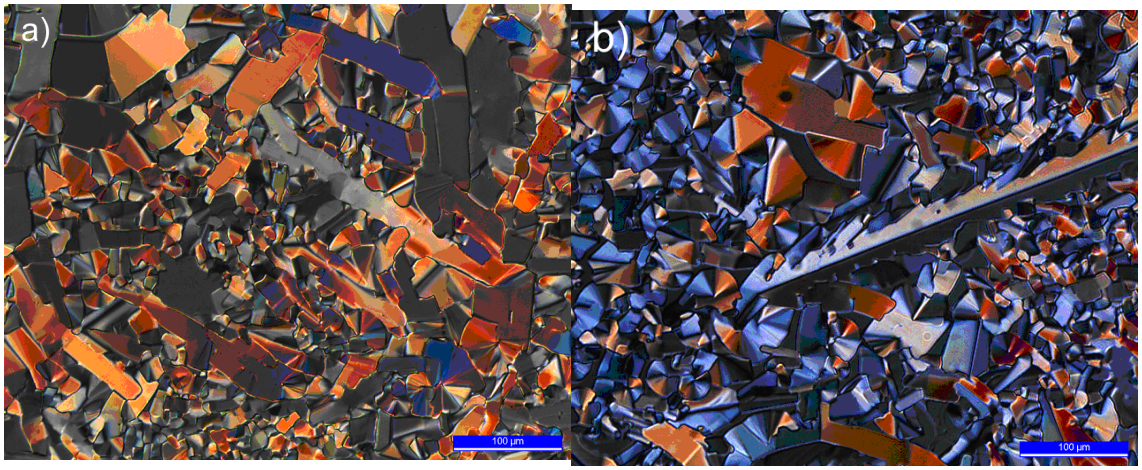

Figure S24. PLOM micrographs of two different regions of the sample 7BP10 at 72 °C (top) and at room temperature (bottom). The metric bar corresponds to 100 µm (coloured version of Figure 9).

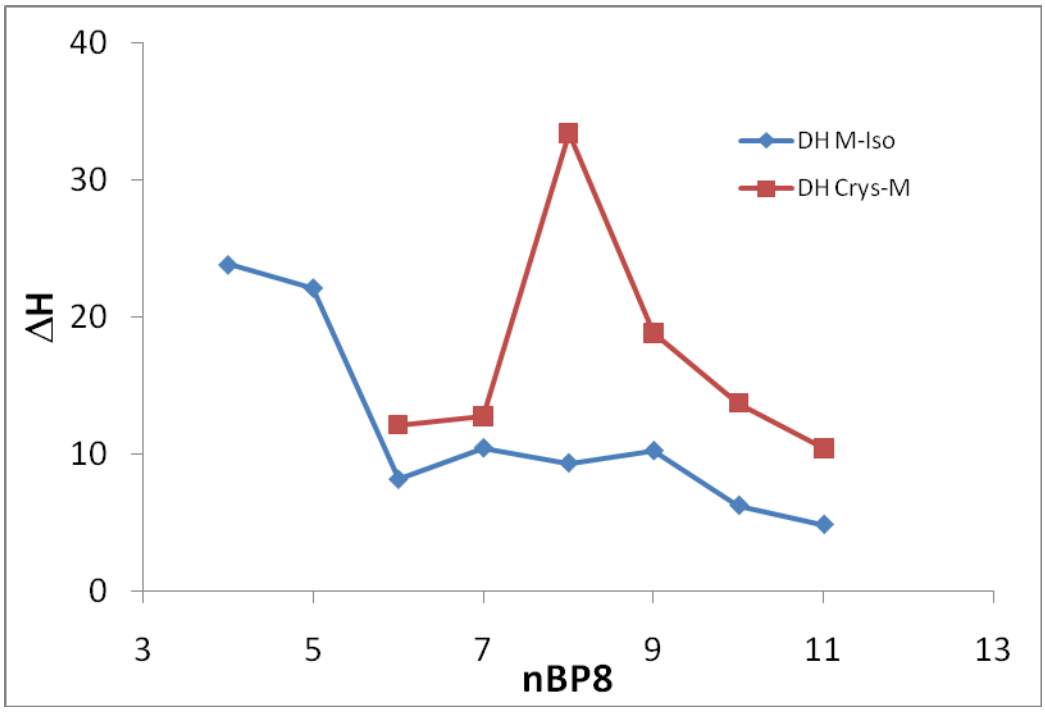

Figure S25. Comparison of the enthalpies of transition, ΔH, for the series nBP8, as a function of n. M-Iso refers to the clearing point (isotropization) while Crys-M to the transition from the crystal into the mesophase.

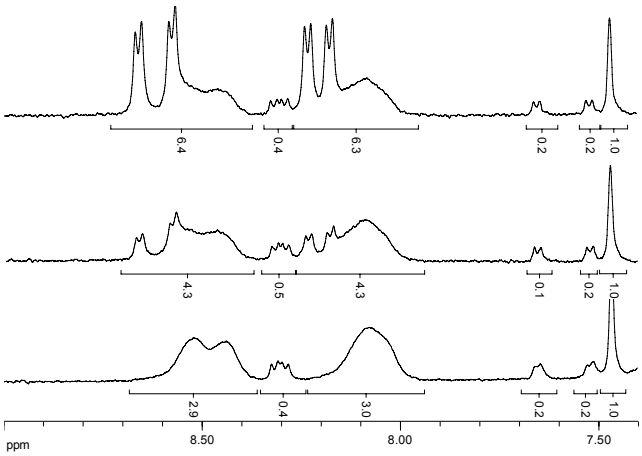

Figure S26a ^{1}H NMR spectra (400 MHz, C_6D_6) of 3BP11, upper phase. From top to bottom: after 15 min., after 3 h, after 24 h. Resonance at 7.47 is the solvent ^{13}C satellite.

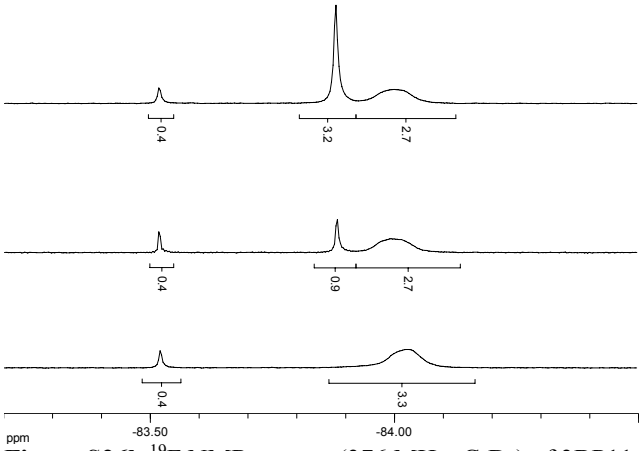

Figure S26b ^{19}F NMR spectra (376 MHz, C_6D_6) of 3BP11, upper phase. From top to bottom: after 15 min., after 3 h, after 24 h.

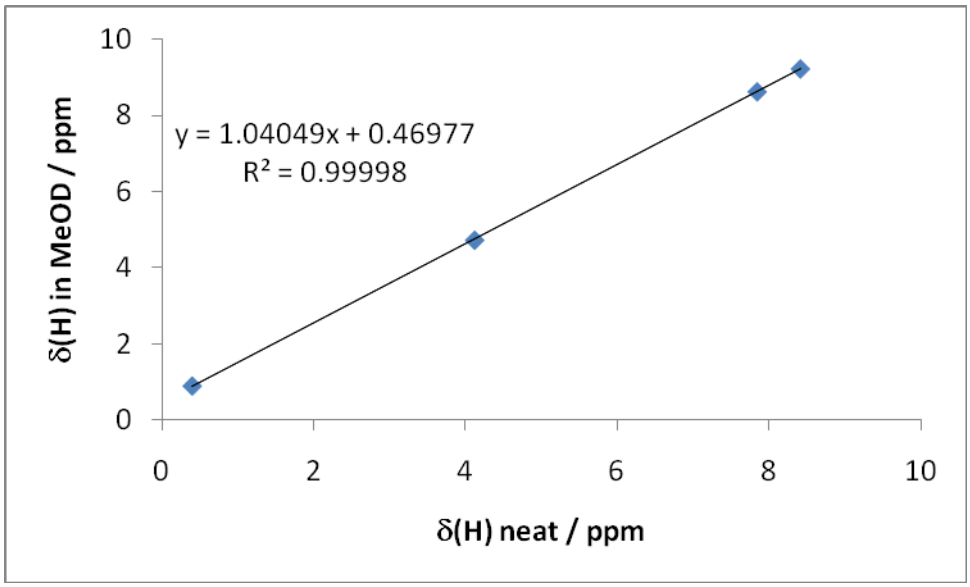

Figure S27. Correlation between ^{1}H chemical shifts of 3BP11 neat vs methanol solution.

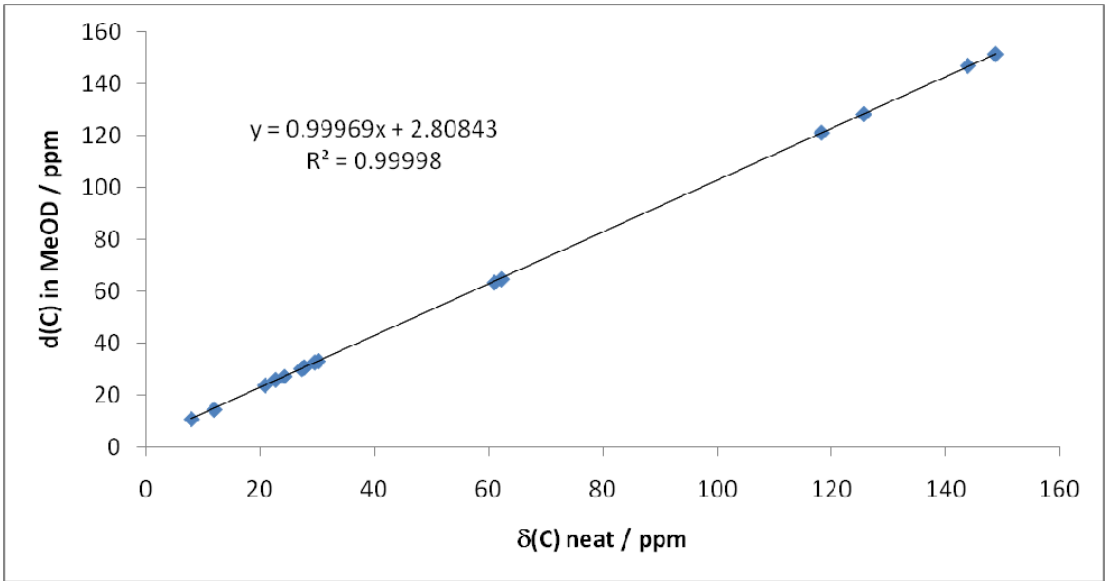

Figure S28. Correlation between ^{13}C chemical shifts of 3BP11 neat vs methanol solution.

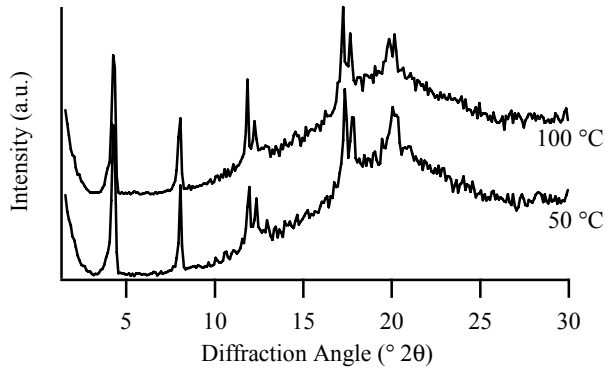

Figure S29. XRD traces of 8BP11 at 50 and 100 °C.